

Copula-based models for spatially dependent cylindrical data

Francesca Labanca¹, Anna Gottard¹, and Nadja Klein²

¹Department of Statistics, Computer Science, Applications, University of Florence, Florence, Italy

²Scientific Computing Center, Karlsruhe Institute of Technology, Karlsruhe, Germany

Abstract

Cylindrical data frequently arise across various scientific disciplines, including meteorology (e.g., wind direction and speed), oceanography (e.g., marine current direction and speed or wave heights), ecology (e.g., telemetry), and medicine (e.g., seasonality and intensity in disease onset). Such data often occur as spatially correlated series of intensities and angles, thereby representing dependent bivariate response vectors of linear and circular components. To accommodate both the circular-linear dependence and spatial autocorrelation, while remaining flexible in marginal specifications, copula-based models for cylindrical data have been developed in the literature. However, existing approaches typically treat the copula parameters as constants unrelated to covariates, and regression specifications for marginal distributions are frequently restricted to linear predictors, thereby ignoring spatial correlation. In this work, we propose a structured additive conditional copula regression model for cylindrical data. The circular component is modeled using a wrapped Gaussian process, and the linear component follows a distributional regression model. Both components allow for the inclusion of linear covariate effects. Furthermore, by leveraging the empirical equivalence between Gaussian random fields (GRFs) and Gaussian Markov random fields, our approach avoids the computational burden typically associated with GRFs, while simultaneously allowing for non-stationarity in the covariance structure. Posterior estimation is performed via Markov chain Monte Carlo simulation. We evaluate the proposed model in a simulation study and subsequently in an analysis of wind directions and speed in Germany.

Keywords: Bayesian inference; Dependence structure; Gaussian (Markov) random fields; Non-stationary spatial process; Wrapped Gaussian process.

Corresponding author: Prof. Dr. Nadja Klein, Scientific Computing Center, Karlsruhe Institute of Technology, Zirkel 2, 76131 Karlsruhe, Germany, nadja.klein@kit.edu.

Acknowledgments: The work of Nadja Klein was supported by the German Research Foundation (Deutsche Forschungsgemeinschaft, DFG) through the Emmy Noether grant KL3037/1-1 and the TRR391 within the project A07, grant number 520388526. The first and second authors were partially supported by the MUR-PRIN grant 2022 SMNNKY, CUP B53D23009470006, by Next Generation EU, Mission 4, Component 2, and the MUR Dept. of Excellence project 2023-2027 ReDS 'Rethinking Data Science' - University of Florence, the European Union - NextGenerationEU - National Recovery.

1 Introduction

Cylindrical data arise when observations involve pairs of a *circular* (an angle with domain in $[0, 2\pi]$), non-Euclidean), and a *linear* variable (such as intensities with domain in a subset of \mathbb{R} , Euclidean). They appear across several scientific disciplines, including meteorology, ecology, medicine, and biometrics. Common examples include wind direction and speed from wind profilers (Carta et al., 2009), wave direction and height from deterministic wave models, and marine current direction and speed recorded by high-frequency radar networks (Meilán-Vila et al., 2021; Lagona and Minigione, 2025). Other applications include animal movement telemetry and the study of seasonality in disease onset (Mastrantonio, 2022; Hodel and Fieberg, 2022). Further applications can be found in Pewsey and García-Portugués (2021). In many environmental and ecological studies, cylindrical data form spatially correlated series, bivariate vectors of angles and intensities observed at different sites (e.g., Lagona, 2018). A key challenge lies in jointly modeling these variables by defining probability distributions that capture angular–linear dependence and potential temporal correlation, while remaining flexible yet parsimonious. Existing approaches use copula-based constructions (Johnson and Wehrly, 1978; Lagona, 2019), circular distributions based on trigonometric sums (Fernández-Durán, 2007), and circulas, the analogue of copulas for directional data (Jones et al., 2015). Recent work introduced circular analogues of Fréchet–Hoeffding bounds for toroidal variables (Ogata, 2023), but extensions to cylindrical or multivariate cases remain unexplored.

We propose a Bayesian copula-based model for cylindrical data that addresses these challenges. Unlike approaches that define the joint distribution directly on the cylinder, we adopt a wrapped approach in its most general form (Mardia and Jupp, 2000), which naturally yields the partially wrapped version on the cylinder $\mathbb{S}^1 \times \mathbb{R}$ by wrapping only the first component around the circle. Our key idea is to recover the latent winding number and model the unwrapped spatial process via copulas, thereby avoiding partial periodicity and enabling flexible dependence modeling. While covariate-dependent copulas for linear data are well-studied (e.g., Acar et al., 2011; Klein and Kneib, 2016b; Vatter and Nagler, 2018), their extension to cylindrical settings remains unexplored. Our work fills this gap by incorporating covariate effects into the copula parameter. We focus on parametric copula families to assess tail behaviour: Gaussian (symmetric, tail-independent), Clayton (lower-tail), and Gumbel (upper-tail). Spatial dependence is introduced through latent Gaussian random fields represented via stochastic partial differential equations (SPDEs), allowing efficient inference via sparse precision matrices (Lindgren et al., 2011; Miller et al., 2020). By exploiting these latent fields and using copulas to govern the dependence between the unwrapped circular and the linear variable, we obtain flexible bivariate distributions on \mathbb{R}^2 . We illustrate the methodology on wind direction and speed data from the Deutscher Wetterdienst (DWD), accounting for spatial dependence, circular–linear marginals, and covariate-driven copula structures. Unlike usual Gaussian-based approaches (Lang et al., 2019), our framework accommodates non-Gaussian margins and allows for non-linear dependence between the circular and linear variables. Although our application focuses on wind, the framework generalizes to any spatial circular–linear data.

The remainder of the paper is structured as follows. In Sec. 2 we introduce the partially wrapped conditional copula regression models, with details about the main building blocks. Sec. 3 presents

Bayesian inference in the proposed partially wrapped conditional copula regression models. Sections 4 and 5 empirically study our approach through simulations and its application to wind data. Sec. 6 concludes and discusses directions of future research.

2 Bivariate conditional copula models with mixed circular-linear marginals

In this section, we outline our model specification and exemplify it along with specific choices relevant to our application in Sec. 5.

Our focus is on bivariate spatial data $(\varphi_1(\mathbf{s}), Y_2(\mathbf{s}))^\top$, where $\varphi_1(\mathbf{s})$ and $Y_2(\mathbf{s})$ denote spatial stochastic processes observed at locations $\mathbf{s} \in \mathcal{D} \subset \mathbb{R}^2$. Without loss of generality, we assume that $\varphi_1(\mathbf{s})$ is a circular response taking values in $[0, 2\pi)$, and $Y_2(\mathbf{s})$ is a linear continuous response taking values in \mathbb{R} . Following the partially wrapped approach of Jona-Lasinio et al. (2012), we define $\varphi_1(\mathbf{s})$ as the wrapped counterpart of an underlying unwrapped linear spatial process $Y_1(\mathbf{s}) \in \mathbb{R}$ for all \mathbf{s} ,

$$\varphi_1(\mathbf{s}) = Y_1(\mathbf{s}) \bmod 2\pi. \quad (1)$$

Knowledge of $\varphi_1(\mathbf{s})$ alone is insufficient to recover the linear representation $Y_1(\mathbf{s})$. To address this, we introduce a latent *winding number* process $k(\mathbf{s}) \in \mathbb{Z}$ for all \mathbf{s} , such that $Y_1(\mathbf{s}) = \varphi_1(\mathbf{s}) + 2\pi k(\mathbf{s})$. This identity establishes a one-to-one correspondence between $Y_1(\mathbf{s})$ and the pair $(\varphi_1(\mathbf{s}), k(\mathbf{s}))^\top$. To model the joint behavior of $(\varphi_1(\mathbf{s}), Y_2(\mathbf{s}))^\top$, we adopt a data augmentation strategy and instead model $\mathbf{Y}(\mathbf{s}) = (Y_1(\mathbf{s}), Y_2(\mathbf{s}))^\top = (\varphi_1(\mathbf{s}) + 2\pi k(\mathbf{s}), Y_2(\mathbf{s}))^\top$.

To build a flexible joint regression model for $\mathbf{Y}(\mathbf{s})$ given some covariates $\mathbf{z}(\mathbf{s}) \in \mathbb{R}^p$, we adopt the conditional copula regression framework of Klein and Kneib (2016b), which enables flexible distributional regression by decoupling the specification of marginal distributions of $Y_1(\mathbf{s}), Y_2(\mathbf{s})$ from the modeling of the dependence between the two. The approach relies on Sklar's theorem, which states that we can write the joint conditional distribution $F_{1,2}(y_1(\mathbf{s}), y_2(\mathbf{s}) \mid \mathbf{z}(\mathbf{s}))$ of $\mathbf{Y}(\mathbf{s})$ given $\mathbf{z}(\mathbf{s})$ and \mathbf{s} as

$$F_{1,2}(y_1(\mathbf{s}), y_2(\mathbf{s}) \mid \mathbf{z}(\mathbf{s})) = C(F_1(y_1(\mathbf{s}) \mid \mathbf{z}(\mathbf{s})), F_2(y_2(\mathbf{s}) \mid \mathbf{z}(\mathbf{s})) \mid \mathbf{z}(\mathbf{s})),$$

where $F_1(\cdot \mid \mathbf{z})$ and $F_2(\cdot \mid \mathbf{z}(\mathbf{s}))$ are the marginal conditional cumulative distribution functions (CDFs) of $Y_1(\mathbf{s}), Y_2(\mathbf{s})$, and $C(\cdot, \cdot \mid \mathbf{z}(\mathbf{s}))$ is the covariate-dependent copula function. Assuming $\mathbf{Y}(\mathbf{s})$ to be continuous, this representation is unique and the marginal densities $p_1(y_1(\mathbf{s}) \mid \mathbf{z}(\mathbf{s})), p_2(y_2(\mathbf{s}) \mid \mathbf{z})$, and the copula density $c(\cdot, \cdot \mid \mathbf{z}(\mathbf{s})) = \frac{\partial^2}{\partial y_1(\mathbf{s}) \partial y_2(\mathbf{s})} C(\cdot, \cdot \mid \mathbf{z}(\mathbf{s}))$ exist. Hence, the joint conditional probability density function (PDF) of $\mathbf{Y}(\mathbf{s})$ is

$$p_{1,2}(y_1(\mathbf{s}), y_2(\mathbf{s}) \mid \mathbf{z}(\mathbf{s})) = c(F_1(y_1(\mathbf{s}) \mid \mathbf{z}(\mathbf{s})), F_2(y_2(\mathbf{s}) \mid \mathbf{z}(\mathbf{s})) \mid \mathbf{z}(\mathbf{s})) p_1(y_1(\mathbf{s}) \mid \mathbf{z}(\mathbf{s})) p_2(y_2(\mathbf{s}) \mid \mathbf{z}(\mathbf{s})).$$

The conditional PDF of the partially wrapped (PW) vector $(\varphi_1(\mathbf{s}), Y_2(\mathbf{s}))^\top$ is

$$p_{1,2}^{PW}(\varphi_1(\mathbf{s}), Y_2(\mathbf{s}) \mid \mathbf{z}(\mathbf{s})) = \sum_{k(\mathbf{s}) \in \mathbb{Z}} p_{1,2}(\varphi_1(\mathbf{s}) + 2\pi k(\mathbf{s}), Y_2(\mathbf{s}) \mid \mathbf{z}(\mathbf{s})). \quad (2)$$

see the Supplementary Material (SM) A.1 for details. Furthermore, the marginal PDF p_1 is the joint distribution of $(\varphi_1(\mathbf{s}), k(\mathbf{s}))^\top$, and marginalizing with respect to the winding number $k(\mathbf{s})$ yields the conditional density of $\varphi_1(\mathbf{s})$, as summarized in Lemma 1.

Lemma 1. *The margins of the PW copula model defined in (2) are p_2 and the wrapped counterpart of p_1 , i.e.,*

$$p_1^W(\varphi_1(\mathbf{s}) \mid \mathbf{z}(\mathbf{s})) = \sum_{k(\mathbf{s}) \in \mathbb{Z}} p_1(\varphi_1(\mathbf{s}) + 2\pi k(\mathbf{s}) \mid \mathbf{z}(\mathbf{s})). \quad (3)$$

The proof of Lemma 1 is given in the SM A.2.

As a key advantage, we can model arbitrary marginal distributions and their dependence separately as functions of the covariates. We focus on parametric marginal distributions p_1, p_2 and one-parameter copulas with association parameter ρ . We then model each distributional parameter as a function of covariates and space. Specifically, we are concerned with choosing the following components: (i) a parametric copula; (ii) a parametric conditional PDF for the circular response; (iii) a parametric conditional PDF for the linear response; (iv) predictor specifications for all distribution parameters; and (v) a spatial specification that allows for nonstationarity in both the mean and covariance.

Dependence structure To capture different dependence structures, we use the Gaussian, Clayton, and Gumbel copulas (see Table S3, SM B). The Gaussian copula is radially symmetric and exhibits no tail dependence, implying independence in the limit. Within the Archimedean class, the Clayton copula models lower-tail dependence with coefficient $2^{-1/\rho}$, whereas the Gumbel copula captures upper-tail dependence with coefficient $2 - 2^{1/\rho}$. Each is fully specified by ρ , with different admissible ranges. Rotated Archimedean copulas can model negative dependence, but we omit details here, as they did not yield reasonable fits for our application. To incorporate covariate effects, we let $\rho(\mathbf{s}) = h_\rho(\eta_\rho(\mathbf{s}))$, where $h_\rho(\cdot)$ is a bijective function ensuring parameter constraints and $\eta_\rho(\mathbf{s})$ is an unrestricted predictor specified later on. For further details on copula families and dependence properties, we refer to Nelsen (2006).

Modeling the marginal distribution of $\varphi_1(\mathbf{s})$ Among wrapped distributions, the wrapped normal (WN) is a common choice because it links the circular response to an underlying linear Gaussian process (GP), allowing coherent spatial and regression structures (Jona-Lasinio et al., 2012; Marques et al., 2022). Consequently, we choose p_1^W to be a WN distribution induced by $\gamma_1^*(\mathbf{s}) \sim \text{GP}(\mu_{\gamma_1}(\mathbf{s}), \mathcal{K}_1(\mathbf{s}, \mathbf{s}'))$ with mean and variance function $\mu_{\gamma_1}(\mathbf{s}), \mathcal{K}_1(\mathbf{s}, \mathbf{s}')$, respectively. We also consider a white noise process $\epsilon(\mathbf{s})$, modeling measurement error or microscale variation, with independent and identically distributed (i.i.d.) realizations as $N(0, \varsigma_1^2)$. Hence, defining $\gamma_1(\mathbf{s}) \sim \text{GP}(0, \mathcal{K}_1(\mathbf{s}, \mathbf{s}'))$ a zero-mean GP, $\varphi_1(\mathbf{s}) = \mu_{\gamma_1}(\mathbf{s}) + \gamma_1(\mathbf{s}) + \epsilon \pmod{2\pi}$ follows a Wrapped Gaussian process (WGP) with the same mean and covariance function of $\gamma_1^*(\mathbf{s})$. We define the model for the circular random vector $\boldsymbol{\varphi}_1 = (\varphi_1(\mathbf{s}_1), \varphi_1(\mathbf{s}_2), \dots, \varphi_1(\mathbf{s}_n))^\top$ at some specific locations $\mathbf{s}_1, \mathbf{s}_2, \dots, \mathbf{s}_n$ in $\mathcal{D} \subset \mathbb{R}^2$, as

$$\boldsymbol{\varphi}_1 \mid \boldsymbol{\mu}_{\gamma_1}, \gamma_1, \varsigma_1^2 \sim \text{WN}(\boldsymbol{\mu}_{\gamma_1} + \boldsymbol{\gamma}_1, \varsigma_1^2 \mathbf{I}) \quad \text{and} \quad \boldsymbol{\gamma}_1(\mathbf{s}) \sim \text{GP}(0, \mathcal{K}_1(\mathbf{s}, \mathbf{s}')), \quad (4)$$

with the mean vector $\boldsymbol{\mu}_{\gamma_1} = (\mu_{\gamma_1}(\mathbf{s}_1), \mu_{\gamma_1}(\mathbf{s}_2), \dots, \mu_{\gamma_1}(\mathbf{s}_n))^\top$, $\boldsymbol{\gamma}_1 = (\gamma_1(\mathbf{s}_1), \gamma_1(\mathbf{s}_2), \dots, \gamma_1(\mathbf{s}_n))^\top$, and \mathbf{I} the $n \times n$ identity matrix. We denote by $h_{\mu_1}(\cdot)$, $h_{\kappa_1}(\cdot)$, and $h_{\tau_1}(\cdot)$, the elementwise mean, spatial-range-related, and marginal-variance-related parameter response functions. We use the identity for $h_{\mu_1}(\cdot)$ and the exponential the others to ensure positivity of κ_1, τ_1 . Details on the spatial dependence modeling and the corresponding predictors, $\eta_{\mu_1}(\mathbf{s}_i), \eta_{\kappa_1}(\mathbf{s}_i), \eta_{\tau_1}(\mathbf{s}_i)$, are described later in this section.

Modeling the marginal distribution of $Y_2(\mathbf{s})$ The distributional choice for the linear margin should be application-specific. The log-normal distribution provides a reasonable fit to the data. We define $Y_2(\mathbf{s})$ as the log-transformed sum of $\gamma_2^*(\mathbf{s}) \sim \text{GP}(\mu_2(\mathbf{s}), \mathcal{K}_2(\mathbf{s}, \mathbf{s}'))$ and white noise $\epsilon \sim N(0, \varsigma_2^2)$. Analogously to what proposed for $\varphi_1(\mathbf{s})$, we define the model for the linear random vector $\mathbf{Y}_2 = (Y_2(\mathbf{s}_1), Y_2(\mathbf{s}_2), \dots, Y_2(\mathbf{s}_n))^\top$ as

$$\mathbf{Y}_2 \mid \boldsymbol{\mu}_{\gamma_2}, \boldsymbol{\gamma}_2, \varsigma_2^2 \sim \text{LN}(\boldsymbol{\mu}_{\gamma_2} + \boldsymbol{\gamma}_2, \varsigma_2^2 \mathbf{I}) \quad \text{and} \quad \boldsymbol{\gamma}_2(\mathbf{s}) \sim \text{GP}(0, \mathcal{K}_2(\mathbf{s}, \mathbf{s}')) , \quad (5)$$

with $\boldsymbol{\mu}_{\gamma_2} = (\mu_{\gamma_2}(\mathbf{s}_1), \mu_{\gamma_2}(\mathbf{s}_2), \dots, \mu_{\gamma_2}(\mathbf{s}_n))^\top$ and $\boldsymbol{\gamma}_2 = (\gamma_2(\mathbf{s}_1), \gamma_2(\mathbf{s}_2), \dots, \gamma_2(\mathbf{s}_n))^\top$. We denote h_{μ_2} , h_{κ_2} , and h_{τ_2} the elementwise mean, spatial-range-related, and marginal-variance-related parameter response functions. We use the identity for the first one, and the exponential for the remaining, to ensure positivity of κ_2, τ_2 . Details about the spatial dependence modeling are given below. The corresponding predictors are $\eta_{\mu_2}(\mathbf{s}_i), \eta_{\kappa_2}(\mathbf{s}_i), \eta_{\tau_2}(\mathbf{s}_i)$.

Predictor specifications To account for potential covariates and the spatial dependence in the mean and in the covariance functions, we assume linear GPs with $\mu_{\gamma_1}(\mathbf{s}) = \beta_{\mu_1,0} + \mathbf{z}_\beta(\mathbf{s})\boldsymbol{\beta}_{\mu_1,1}$ and $\mu_{\gamma_2}(\mathbf{s}) = \beta_{\mu_2,0} + \mathbf{z}_\beta(\mathbf{s})\boldsymbol{\beta}_{\mu_2,1}$ as mean functions and the following predictor specifications for distributional parameters of the joint PDF,

$$\begin{aligned} \eta_{\mu_1}(\mathbf{s}) &= \beta_{\mu_1,0} + \mathbf{z}_\beta(\mathbf{s})\boldsymbol{\beta}_{\mu_1,1} + \gamma_1(\mathbf{s}, \mathbf{z}_\kappa(\mathbf{s})), & \eta_{\mu_2}(\mathbf{s}) &= \beta_{\mu_2,0} + \mathbf{z}_\beta(\mathbf{s})\boldsymbol{\beta}_{\mu_2,1} + \gamma_2(\mathbf{s}, \mathbf{z}_\kappa(\mathbf{s})), \\ \eta_{\kappa_1}(\mathbf{s}) &= \theta_{\kappa_1,0} + \mathbf{z}_\kappa(\mathbf{s})\boldsymbol{\theta}_{\kappa_1,1}, & \eta_{\kappa_2}(\mathbf{s}) &= \theta_{\kappa_2,0} + \mathbf{z}_\kappa(\mathbf{s})\boldsymbol{\theta}_{\kappa_2,1}, \\ \eta_{\tau_1}(\mathbf{s}) &= \theta_{\tau_1,0}, & \eta_{\tau_2}(\mathbf{s}) &= \theta_{\tau_2,0}, \\ \eta_\rho(\mathbf{s}) &= \beta_{\rho,0} + \mathbf{z}_\rho(\mathbf{s})\boldsymbol{\beta}_{\rho,1}, \end{aligned}$$

where $\beta_{\mu_1,0}, \beta_{\mu_2,0}, \beta_{\rho,0}, \theta_{\tau_1,0}, \theta_{\tau_2,0}$ are intercept terms, $\boldsymbol{\beta}_{\mu_1,1}, \boldsymbol{\beta}_{\mu_2,1}, \boldsymbol{\beta}_{\rho,1}, \boldsymbol{\theta}_{\kappa_1,1}, \boldsymbol{\theta}_{\kappa_2,1}$ are regression coefficient vectors for the covariate effects $\mathbf{z}_\beta(\mathbf{s})$ (marginal means), $\mathbf{z}_\rho(\mathbf{s})$ (dependence parameter), and $\mathbf{z}_\kappa(\mathbf{s})$ (spatial range). The spatial effects $\boldsymbol{\gamma}_1, \boldsymbol{\gamma}_2$ are zero-mean Gaussian Markov random fields (GMRFs) with a non-stationary covariance function, as described later on. The proposed framework allows nonlinear effects both in the margins and the dependence structure. This flexibility parallels that of structured additive predictors (see Wood, 2017, for further details). Given the limited sample size in our application, we focus on linear covariate effects and the flexible modeling of spatial effects. In this regard, we found it sufficient to model $\kappa_1(\mathbf{s}), \kappa_2(\mathbf{s})$ while keeping τ_1 and τ_2 constant in our application.

Modeling spatial effects A Gaussian random field (GRF) is defined as a continuously indexed spatial process with all finite-dimensional vectors multivariate Gaussian. Following Lindgren et al. (2011), expressing a GRFs through an SPDEs allow modeling the spatial effects as a random field defined in continuous space, while enabling efficient computation via discrete GMRFs. Specifically, the stationary Matérn GRF $\gamma(\mathbf{s})$ with $\mathbf{s} \in \mathbb{R}^2$ arises as the solution to the SPDE

$$(\kappa^2 - \Delta)^{\alpha_\nu/2}(\tau \gamma(\mathbf{s})) = W(\mathbf{s}),$$

where W is Gaussian white noise, Δ is the Laplacian, $\kappa > 0$ controls spatial range ϱ , that is the distance at which correlation decays to 0.05, $\tau > 0$ is related to the marginal variance σ^2 , and $\nu > 0$ controls the smoothness. The stationary solution has Matérn covariance

$$\mathcal{K}(\mathbf{s}, \mathbf{s}') = \sigma^2 \frac{1}{2^{\nu-1} \Gamma(\nu)} (\kappa h(\mathbf{s}, \mathbf{s}'))^\nu K_\nu(\kappa h(\mathbf{s}, \mathbf{s}')) , \quad (6)$$

with $h(\mathbf{s}, \mathbf{s}') = \|\mathbf{s} - \mathbf{s}'\|$, and K_ν the modified Bessel function. The SPDE and Matérn parameters are coupled. Specifically, the Matérn smoothness parameter is $\nu = \alpha_\nu - 1$, and the variance σ^2 is proportional to $\tau^{-2} \kappa^{-2\nu}$. Nonstationarity arises by letting $\tau(\mathbf{s})$ and $\kappa(\mathbf{s})$ to vary smoothly over space (Ingebrigtsen et al., 2015). Recent work by Bolin and Kirchner (2020) extends the SPDE approach to fractional powers $\alpha_\nu > 1$, but only in the stationary case. Nonetheless, a closed-form expression for the GMRF precision matrix as a function of κ and τ is available only for $\nu = 1$ (i.e., $\alpha_\nu = 2$). For this reason, we set $\nu = 1$ throughout. For each GRF $\gamma_\ell(\mathbf{s})$ in the two margins, $\ell \in \{1, 2\}$, we thus specify the log-linear models

$$\log \tau_\ell(\mathbf{s}) = \theta_{\tau_\ell,0}, \quad \log \kappa_\ell(\mathbf{s}) = \theta_{\kappa_\ell,0} + \mathbf{z}_\kappa(\mathbf{s}) \boldsymbol{\theta}_{\kappa_\ell,1}, \quad (7)$$

where $\mathbf{z}_\kappa(\mathbf{s})$ collects covariates driving local variation and $\boldsymbol{\theta}_{\kappa_\ell,1}$ are regression coefficients. The parameters $\theta_{\tau_\ell,0}$ and $\theta_{\kappa_\ell,0}$ correspond to the stationary baseline. Provided $\kappa_\ell(\mathbf{s})$ varies smoothly, the SPDE admits a local Matérn interpretation via nominal approximations

$$\varrho_\ell(\mathbf{s}) \approx \frac{\sqrt{8\nu}}{\kappa_\ell(\mathbf{s})}, \quad \sigma_\ell^2(\mathbf{s}) \approx \frac{\Gamma(\nu)}{\Gamma(\alpha_\nu) 4\pi \kappa_\ell(\mathbf{s})^{2\nu} \tau_\ell^2}. \quad (8)$$

A GMRF approximation is obtained via the finite element method (FEM). The domain is triangulated into M nodes, and the GRF is approximated by $\gamma_\ell(\mathbf{s}) = \sum_{m=1}^M \psi_m(\mathbf{s}) \gamma_{\mu_\ell, m}$, with $\{\psi_m(\mathbf{s})\}_{m=1}^M$ piecewise linear basis functions with compact support, whose accuracy improves with finer meshes, while the Markov property ensures computational tractability.

3 Bayesian inference

This section details the prior specification, hyperparameter choices, and posterior evaluation of the proposed hierarchical model. Throughout, we denote the matrices of spatial covariates in the mean, and copula predictors as $\mathbf{Z}_\beta = (\mathbf{z}_\beta(\mathbf{s}_1), \dots, \mathbf{z}_\beta(\mathbf{s}_n))^\top$, and $\mathbf{Z}_\rho = (\mathbf{z}_\rho(\mathbf{s}_1), \dots, \mathbf{z}_\rho(\mathbf{s}_n))^\top$, respectively. Following what stated in the previous section, each GRF is approximated through a finite element

basis expansion with piecewise linear basis functions $\{\psi_m(\mathbf{s})\}_{m=1}^M$ and Gaussian weights $\boldsymbol{\gamma}_{\mu_\ell} = (\gamma_{\mu_\ell,1}, \dots, \gamma_{\mu_\ell,M})^\top$ for $\ell = 1, 2$. This yields two GMRFs characterized by the hyperparameter vector $\boldsymbol{\theta}_\ell = (\theta_{\tau_\ell,0}, \theta_{\kappa_\ell,0}, \boldsymbol{\theta}_{\kappa_\ell,1}^\top)^\top$. We collect the basis functions in $\boldsymbol{\psi}(\mathbf{s}) = (\psi_1(\mathbf{s}), \dots, \psi_M(\mathbf{s}))^\top$ and define the matrix $\boldsymbol{\psi} = (\boldsymbol{\psi}(\mathbf{s}_1), \dots, \boldsymbol{\psi}(\mathbf{s}_n))^\top$. The model parameters are grouped as $\boldsymbol{\vartheta}_1 = (\beta_{\mu_1,0}, \boldsymbol{\beta}_{\mu_1,1}^\top, \boldsymbol{\gamma}_{\mu_1}^\top, \boldsymbol{\xi}_{\mu_1}^2)^\top$, $\boldsymbol{\vartheta}_2 = (\beta_{\mu_2,0}, \boldsymbol{\beta}_{\mu_2,1}^\top, \boldsymbol{\gamma}_{\mu_2}^\top, \boldsymbol{\xi}_{\mu_2}^2)^\top$, and $\boldsymbol{\vartheta}_\rho = (\beta_{\rho,0}, \boldsymbol{\beta}_\rho^\top)^\top$ for the two marginal and the copula components. A graphical illustration of the full hierarchical models is shown in Figure 1.

3.1 Prior specifications

We adopt conjugate priors whenever possible. We assign Gaussian priors for the regression coefficients and inverse gamma (IG) priors for their variances. For the overall level of the mean and copula predictors, $\beta_{\mu_\ell,0}$, $\beta_{\rho,0}$, we choose Gaussian priors with zero mean and large variances as a weakly informative prior on the log-scale. For the remaining coefficients, $\boldsymbol{\beta}_{\mu_\ell,1}$ and $\boldsymbol{\beta}_{\rho,1}$, we assume independent, homoscedastic priors, with zero-mean Gaussian distributions with variances $\boldsymbol{\xi}_{\mu_\ell}^2$ and $\boldsymbol{\xi}_\rho^2$, respectively. The error variance $\boldsymbol{\xi}_\ell^2$ and the scaling variances $\boldsymbol{\xi}_{\mu_\ell}^2$ and $\boldsymbol{\xi}_\rho^2$ use IG priors with shape and scale equal to 0.001 to obtain a data-driven smoothness. Discretization of the spatial domain yields Gaussian vectors $\boldsymbol{\gamma}_{\mu_\ell}$ with a sparse precision matrix $\mathbf{Q}(\boldsymbol{\theta}_\ell)$, depending on the FEM and on the spatial regression coefficients $\boldsymbol{\theta}_\ell$, as defined in (7). More details about the construction of $\mathbf{Q}(\boldsymbol{\theta}_\ell)$ can be found in the SM C.2.

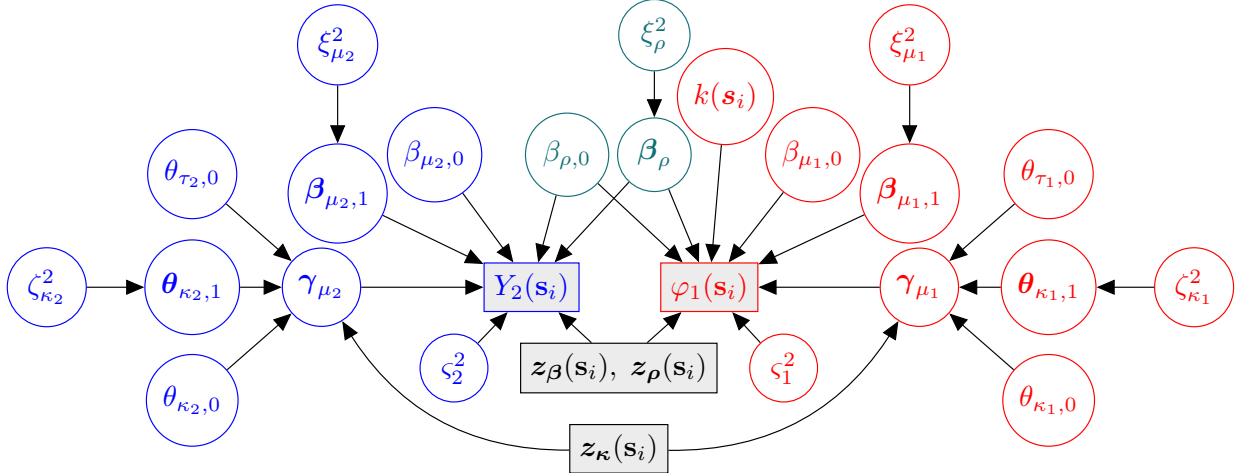


Figure 1: Graphical representation of the full hierarchical model. Shown are the spatially dependent covariates (grey), the model parameters and data $\{\varphi_1(\mathbf{s}_i)\}_{i=1}^n$ related to the wrapped circular random variable red), the model parameters and data $\{y_2(\mathbf{s}_i)\}_{i=1}^n$ related to the linear random variable (blue), and the copula-parameters (petrol).

Here, $\theta_{\tau_\ell,0}$ and $\theta_{\kappa_\ell,0}$ represent the stationary baseline, with (8) giving their local interpretation

of range and marginal variance. We assign to them independent uniform priors, chosen to yield interpretable ranges for the marginal variance and correlation range. To control deviations from stationarity, we assign a standard Gaussian prior to the spatial coefficients $\boldsymbol{\theta}_{\kappa_\ell,1}$, with smoothing variance $\zeta_{\kappa_\ell}^2$ endowed with a penalized complexity (PC) prior (Simpson et al., 2017). The PC prior provides a principled mechanism to penalize model complexity by shrinking towards a predefined *base model*, here, a stationary covariance function. Hence, non-stationarity is introduced only when supported by the data, ensuring parsimony and interpretability. Under the PC prior, a model component is treated as a flexible extension of a simpler base model, and the prior density decreases exponentially with the Kullback–Leibler divergence from the base, thereby enforcing a constant-rate penalization of complexity. The guiding principles are listed in SM D. Klein and Kneib (2016a) proved that if the base model is obtainable for $\xi_{\kappa_\ell}^2 \rightarrow 0$, i.e., $\boldsymbol{\theta}_{\kappa_\ell,1} = \mathbf{0}$ in our case, and thus, the field predictor η_{κ_ℓ} is constant, if $\xi_{\kappa_\ell}^2$ -prior is constructed according to the PC-prior principles, $\xi_{\kappa_\ell}^2$ follows a Weibull distribution with shape 1/2 and scale λ , i.e., $\xi_{\kappa_\ell}^2 \sim \text{Weibull}(\frac{1}{2}, \lambda)$. The rate parameter λ is determined via a user-defined tail probability condition that encodes prior beliefs on the plausible degree of non-stationarity and is elicited as described later. A prior sensitivity analysis for $\xi_{\mu_1}^2$ and $\zeta_{\mu_1}^2$ in the circular marginal model can be found in Marques et al. (2022).

For the latent winding numbers $k(\mathbf{s}_i) \in \mathbb{Z}$, assigning a prior over the full integer domain is computationally intractable. Following Jona-Lasinio et al. (2020) and Marques et al. (2022), we adopt a truncated uniform prior with restricted support, i.e., $p(k_i) = \frac{1}{3}\mathbf{1}_{\{k_i \in \{-1, 0, 1\}\}}$, which provides a practical and accurate approximation for the univariate WN distribution (Kurz et al., 2014). Thus, the resulting hierarchical model is the partially wrapped copula (PWC) model with wrapped normal and log-normal margins, specified as

$$\begin{aligned}
& (\varphi_1(\mathbf{s}_i), Y_2(\mathbf{s}_i))^\top \mid \mathbf{z}_\beta(\mathbf{s}_i), \mathbf{z}_\rho(\mathbf{s}_i), \vartheta_1, \vartheta_2, \vartheta_\rho \sim \text{PWC}(\vartheta_1, \vartheta_2, \vartheta_\rho) \\
& \beta_{\rho,0} \sim N(0, 100), \beta_{\rho,1} \mid \xi_\rho^2 \sim N(\mathbf{0}, \xi_\rho^2 \mathbf{I}), \xi_\rho^2 \sim IG(0.001, 0.001), \\
& \beta_{\mu_\ell,0} \sim N(0, 10), \beta_{\mu_\ell,1} \mid \xi_{\mu_\ell}^2 \sim N(\mathbf{0}, \xi_{\mu_\ell}^2 \mathbf{I}), \xi_{\mu_\ell}^2 \sim IG(0.001, 0.001), \\
& \gamma_{\mu_\ell} \mid z_\kappa(\mathbf{s}_i), \boldsymbol{\theta}_\ell \sim N(\mathbf{0}, \mathbf{Q}^{-1}(\boldsymbol{\theta}_\ell)), \\
& \theta_{\tau_1,0} \sim U(a_{\tau_1}, b_{\tau_1}), \theta_{\tau_2,0} \sim U(a_{\tau_2}, b_{\tau_2}), \\
& \theta_{\kappa_\ell,0} \sim U(a_\kappa, b_\kappa), \theta_{\kappa_\ell,1} \mid \zeta_{\kappa_\ell}^2 \sim N(\mathbf{0}, \zeta_{\kappa_\ell}^2 \mathbf{I}), \zeta_{\kappa_\ell}^2 \sim PC(c, \alpha_\zeta), \\
& \zeta_\ell^2 \sim IG(0.001, 0.001), p(k_i) = \frac{1}{3}\mathbf{1}_{\{k_i \in \{-1, 0, 1\}\}}.
\end{aligned} \tag{9}$$

The specific ranges for uniform priors are described next.

Prior scaling To penalize the non-stationarity in the covariance of the margins, we want the uniform priors to ensure that the spatial ranges and marginal variances fall within predefined intervals. After rescaling the domain, for $\mathcal{D} \subseteq [0, 1]^2$, the spatial ranges are in $[0.01, 1]$ and marginal variances in $[0.01, s_{\max}^2]$, for a chosen $s_{\max}^2 > 0.01$. The latter follows from the nominal approximation in (7), linking $\varrho(\mathbf{s}_i)$ to $\kappa(\mathbf{s}_i)$, and $\sigma(\mathbf{s}_i)$ to $\tau(\mathbf{s}_i)$ and $\kappa(\mathbf{s}_i)$. Hence, $\theta_{\tau_\ell,0} \sim \mathcal{U}(-7 - \log s_{\max}, 0)$, $\theta_{\kappa_\ell,0} \sim \mathcal{U}(1, 6)$. For circular responses, we choose $s_{\max} = 2\pi$, since it reflects the maximal support length. For linear response, we refer to the Beaufort Wind Scale ((0, 31.5] m/s). On a logarithmic scale, this gives

$s_{max} = 3.45$. The scale parameter λ is calibrated by simulation, using the tail bound

$$\Pr \left(\max_{\mathbf{s}_i \in \mathcal{D}} |z_\kappa(\mathbf{s}_i) \boldsymbol{\theta}_{\kappa_\ell}| \leq c \right) \geq 1 - \alpha_\zeta, \quad (10)$$

for user-defined constants $\alpha_\zeta \in (0, 1)$ and $c > 0$, which controls the magnitude of the nonstationary deviation. This ensures that with probability at least $1 - \alpha_\zeta$, the nonstationary effect in the covariance does not exceed the bound c . Under the rescaled domain assumption, based on the range constraint $\rho(\mathbf{s}_i) \in [0.01, 1]$, we choose the bound c as

$$c = \left\lceil \frac{1}{2} \left| \log\left(\frac{\sqrt{8}}{0.01}\right) - \log(\sqrt{8}) \right| \right\rceil. \quad (11)$$

3.2 Likelihood

With the specific choices of copula, and marginal distributions, the joint likelihood of our PWC model for a dataset of n observations $\{y_1(\mathbf{s}_i), \varphi_2(\mathbf{s}_i), \mathbf{z}_\beta(\mathbf{s}_i), \mathbf{z}_\rho(\mathbf{s}_i), \mathbf{s}_i\}_{i=1}^n$ is

$$\begin{aligned} l(\boldsymbol{\vartheta}_1, \boldsymbol{\vartheta}_2, \boldsymbol{\vartheta}_\rho) = \prod_{i=1}^n & c(\Phi(\varphi_1(\mathbf{s}_i) + 2\pi k(\mathbf{s}_i) | z_\beta(\mathbf{s}_i), \boldsymbol{\vartheta}_1), \Phi(\log(y_2(\mathbf{s}_i)) | z_\beta(\mathbf{s}_i), \boldsymbol{\vartheta}_2) | z_\rho(\mathbf{s}_i), \boldsymbol{\vartheta}_\rho) \cdot \\ & \phi(\varphi_1(\mathbf{s}_i) + 2\pi k(\mathbf{s}_i) | z_\beta(\mathbf{s}_i), \boldsymbol{\vartheta}_1) \cdot \frac{1}{y_2(\mathbf{s}_i)} \phi(\log(y_2(\mathbf{s}_i)) | z_\beta(\mathbf{s}_i), \boldsymbol{\vartheta}_2) \end{aligned} \quad (12)$$

where Φ and ϕ are the univariate Gaussian CDF and pdf, with parameters $\boldsymbol{\vartheta}_1$ and $\boldsymbol{\vartheta}_2$.

3.3 Posterior estimation

Posterior estimation in our PWC model becomes tractable by introducing the winding number vector $\mathbf{k} = (k(\mathbf{s}_1), \dots, k(\mathbf{s}_n))^\top$ as a latent variable. Assuming prior independence among model parameters, the log-posterior distribution is

$$\begin{aligned} p(\boldsymbol{\vartheta}_1, \boldsymbol{\vartheta}_2, \boldsymbol{\vartheta}_\rho, \boldsymbol{\theta}_1, \boldsymbol{\theta}_2, \xi_{\mu_1}^2, \xi_{\mu_2}^2, \xi_{\mu_\rho}^2, \zeta_{\kappa_1}^2, \zeta_{\kappa_2}^2 | \mathbf{y}, \boldsymbol{\varphi}, \mathbf{k}, \mathbf{Z}_\beta, \mathbf{Z}_\kappa, \mathbf{Z}_\rho) \propto l(\boldsymbol{\vartheta}_1, \boldsymbol{\vartheta}_2, \boldsymbol{\vartheta}_\rho) \cdot \\ p(\boldsymbol{\beta}_\rho | \xi_\rho^2) p(\xi_\rho^2) \prod_{\ell=1}^2 p(\zeta_\ell^2) p(\boldsymbol{\beta}_{\mu_\ell} | \xi_{\mu_\ell}^2) p(\xi_{\mu_\ell}^2) p(\boldsymbol{\gamma}_{\mu_\ell} | \boldsymbol{\theta}_{\mu_\ell}^2) p(\boldsymbol{\theta}_{\mu_\ell}^2) p(\theta_{\tau_\ell, 0}) p(\theta_{\kappa_\ell, 0}) p(\boldsymbol{\theta}_{\kappa_\ell, 1} | \zeta_{\kappa_\ell}^2) p(\zeta_{\kappa_\ell}^2), \end{aligned}$$

proportional to the likelihood (Sec. 3.2), and the prior distributions (Sec. 3.1).

We develop a two-stage Bayesian approach based on MCMC simulations to estimate the model parameters and hyperparameters. This approach fits the marginal models first and, conditional on the fitted marginals, estimates the copula parameter model. This yields substantial computational savings compared with the joint estimation. Previous work (e.g., Klein and Kneib, 2016b) has shown that this two-step procedure does not substantially underestimate uncertainty compared to the joint estimation. In the first stage, given the latent variables \mathbf{k} , and transforming back the linear one, any standard algorithm for sampling Gaussian process parameters can be used. The posterior for $\boldsymbol{\beta}_{\mu_\ell}, \boldsymbol{\gamma}_{\mu_\ell}$ are sampled via Gibbs, since the full conditionals are wrapped normal and

normal. Using the following vector form of the mean predictors for the two margins, and the copula predictor, $\boldsymbol{\eta}_{\mu_\ell} = \mathbf{1}\beta_{\mu_\ell,0} + \mathbf{Z}_\beta\boldsymbol{\beta}_{\mu_\ell,1} + \boldsymbol{\psi}\gamma_{\mu_\ell}$, $\boldsymbol{\eta}_\rho = \mathbf{1}\beta_{\rho,0} + \mathbf{Z}_\rho\boldsymbol{\beta}_{\rho,1}$, we can explicitly write their full conditional distributions as

$$\begin{aligned}\beta_{\mu_\ell,0} | \cdot &\sim N\left(\left(\frac{n}{\zeta_\ell^2} + \frac{1}{10}\right)^{-1} \left(\frac{n}{\zeta_\ell^2} \mathbf{1}^\top (\tilde{\mathbf{y}}_\ell - \boldsymbol{\eta}_{\mu_\ell} + \mathbf{1}\beta_{\mu_1,0})\right), \left(\frac{n}{\zeta_\ell^2} + \frac{1}{10}\right)^{-1}\right) \\ \boldsymbol{\beta}_{\mu_\ell,1} | \cdot &\sim N\left(\left(\frac{1}{\zeta_\ell^2} \mathbf{Z}_\beta^\top \mathbf{Z}_\beta + \frac{1}{\xi_{\mu_\ell}^2} \mathbf{I}\right)^{-1} \left(\frac{1}{\zeta_\ell^2} \mathbf{Z}_\beta^\top (\tilde{\mathbf{y}}_\ell - \boldsymbol{\eta}_{\mu_\ell} + \mathbf{Z}_\beta\boldsymbol{\beta}_{\mu_\ell,1})\right), \left(\frac{1}{\zeta_\ell^2} \mathbf{Z}_\beta^\top \mathbf{Z}_\beta + \frac{1}{\xi_{\mu_\ell}^2} \mathbf{I}\right)^{-1}\right) \\ \boldsymbol{\gamma}_{\mu_\ell} | \cdot &\sim N\left(\left(\frac{1}{\zeta_\ell^2} \boldsymbol{\psi}^\top \boldsymbol{\psi} + \mathbf{Q}(\boldsymbol{\theta}_\ell)\right)^{-1} \left(\frac{1}{\zeta_\ell^2} \boldsymbol{\psi}^\top (\tilde{\mathbf{y}}_\ell - \boldsymbol{\eta}_{\mu_\ell} + \boldsymbol{\psi}\gamma_{\mu_\ell,1})\right), \left(\frac{1}{\zeta_\ell^2} \boldsymbol{\psi}^\top \boldsymbol{\psi} + \mathbf{Q}(\boldsymbol{\theta}_\ell)\right)^{-1}\right) \\ \zeta_\ell^2 | \cdot &\sim IG\left(\frac{n}{2} + 0.001, \frac{1}{2} (\tilde{\mathbf{y}}_\ell - \boldsymbol{\eta}_{\mu_\ell})^\top (\tilde{\mathbf{y}}_\ell - \boldsymbol{\eta}_{\mu_\ell}) + 0.001\right) \\ \xi_{\mu_\ell}^2 | \cdot &\sim IG\left(\frac{p_{z_\beta}}{2} + 0.001, \frac{1}{2} \boldsymbol{\beta}_{\mu_\ell,1}^\top \boldsymbol{\beta}_{\mu_\ell,1} + 0.001\right) \\ \xi_\rho^2 | \cdot &\sim IG\left(\frac{p_{z_\rho}}{2} + 0.001, \frac{1}{2} \boldsymbol{\beta}_{\rho,1}^\top \boldsymbol{\beta}_{\rho,1} + 0.001\right)\end{aligned}$$

where $\tilde{\mathbf{y}}_1 = \boldsymbol{\varphi}_1 + 2\pi\mathbf{k}$, $\tilde{\mathbf{y}}_2 = \log(\mathbf{y}_2)$ and p_{z_β} , p_{z_ρ} are the covariates number in the mean and in the copula, respectively. See SM C.1 for calculation details. The identifiability challenges of covariance parameters in GRFs are well documented (Tang et al., 2021). These issues arise in our setting as well, and since the components of $\boldsymbol{\theta}_\ell$ exhibit strong posterior correlation, they are updated jointly in a single Metropolis–Hastings block, using the Robust Adaptive Metropolis algorithm (Vihola, 2012) with t-Student proposals. This method adaptively estimates the shape of the target distribution while enforcing a desired acceptance rate. We follow the recommendations of 23.4% as the acceptance rate in multidimensional targets and 44% in unidimensional targets (Gelman et al., 1997) for the GMRF smoothing variances $\zeta_{\kappa_\ell}^2$. To avoid negative invalid proposals, we reparameterize on the log-scale and approximate the log-full conditional $\log p(\log \zeta_{\kappa_\ell}^2 | \cdot)$, rather than $\log p(\zeta_{\kappa_\ell}^2 | \cdot)$. Each latent winding number $k(\mathbf{s}_i)$ is updated at each iteration using a separate Metropolis step. At the t -th iteration, given a current state $k^{[t]}(\mathbf{s}_i)$, the proposal is drawn uniformly from $\{k^{[t]}(\mathbf{s}_i) - 1, k^{[t]}(\mathbf{s}_i), k^{[t]}(\mathbf{s}_i) + 1\}$. Considering the prior choice in Sec. 3.1, the initial values are set as $k^{(0)}(\mathbf{s}_i) = 0$ for all $\mathbf{s}_i \in \mathcal{D}$.

In the second stage, we work with the estimated copula data $\mathbf{u}_1 = (u_1(\mathbf{s}_1), \dots, u_1(\mathbf{s}_n))^\top$, and $\mathbf{u}_2 = (u_2(\mathbf{s}_1), \dots, u_2(\mathbf{s}_n))^\top$ defined as $u_\ell(\mathbf{s}_i) = F_\ell(y_\ell(\mathbf{s}_i) | \widehat{\boldsymbol{\theta}}_\ell)$, $i = 1, \dots, n$, $\ell = 1, 2$, where $\widehat{\boldsymbol{\theta}}_\ell$ are the posterior mean estimates of the parameters for margin ℓ . For sampling the posterior copula regression coefficients, we rely on Metropolis-Hastings steps with Iteratively Weighted Least Squares (IWLS) proposal densities (Klein et al., 2015). The regression coefficients $\boldsymbol{\beta}_\rho^{[t]}$ at the t -th iteration are proposed from $q(\boldsymbol{\beta}_\rho^* | \boldsymbol{\beta}_\rho^{[t]}) = \mathcal{N}(\boldsymbol{\mu}^{[t]}, P^{-1}{}^{[t]})$, with

$$P^{[t]} = \mathbf{Z}_\rho^\top W^{[t]} \mathbf{Z}_\rho + \frac{1}{\xi_\rho^2} \mathbf{I}, \text{ and } \boldsymbol{\mu}^{[t]} = (P^{[t]})^{-1} \mathbf{Z}_\rho^\top W^{[t]} \left(\mathbf{Z}_\rho \boldsymbol{\beta}_\rho^{[t]} + (W^{[t]})^{-1} \mathbf{v}^{[t]} \right),$$

where $\mathbf{W}^{[t]}$ is a working weight matrix having the negative second derivatives of the log-likelihood $\log(l)$ with respect to the predictor $\boldsymbol{\eta}_\rho$ on the diagonal, i.e., $w_{ii} = -\frac{\partial^2}{(\partial \eta_i)^2} \log(l)$ and zeros otherwise; and $\mathbf{v}^{[t]} = \frac{\partial}{\partial \boldsymbol{\eta}} \log(l)$ is the score vector. The working weights and score vector are determined by the chosen copula distribution, thereby ensuring automatic adaptation to the form of the full conditional and eliminating the need for manual tuning.

3.4 Model choice

For model comparison, we rely on the deviance information criterion (DIC) and the Watanabe–Akaike information criterion (WAIC), both of which approximate out-of-sample predictive accuracy and are asymptotically equivalent to leave-one-out cross-validation (see Spiegelhalter et al. (2002); Watanabe and Opper (2010)). Let $\boldsymbol{\vartheta}^{[1]}, \dots, \boldsymbol{\vartheta}^{[T]}$ denote the full parameter vectors sampled via MCMC from the posterior, the DIC is given by $\text{DIC} = \frac{2}{T} \sum_t D(\boldsymbol{\vartheta}^{[t]}) - D(\frac{1}{T} \sum_t \boldsymbol{\vartheta}^{[t]})$ where $D(\boldsymbol{\vartheta}) = -2 \log p(\mathbf{y} \mid \boldsymbol{\vartheta})$. The WAIC is given by $\text{WAIC} = -2(\text{lppd} - p_{\text{WAIC}})$, where $\text{lppd} = \sum_{i=1}^n \log \int p(y_i \mid \boldsymbol{\vartheta}) p(\boldsymbol{\vartheta} \mid \mathbf{y}) d\boldsymbol{\vartheta}$ and $p_{\text{WAIC}} = \sum_{i=1}^n 2 \text{var}_{\boldsymbol{\vartheta}}(\log p(y_i \mid \boldsymbol{\vartheta}))$ (see Gelman et al., 2013; Vehtari et al., 2017). More details are provided in the SM E.

In our application, we use both DIC and WAIC to inform model choice, striking a balance between predictive accuracy and parsimony. Thanks to the limited number of covariates, in the application in Sec. 5, we explore all possible combinations of candidate predictors.

4 Simulation study

We conduct a simulation study to assess the ability of the proposed methodology to identify tail dependence and covariate effects in the copula parameter. Specifically, we compare the performance of three copula families, Gaussian, Clayton, and Gumbel, representing the absence of tail dependence, lower-tail dependence, and upper-tail dependence, respectively, and both, covariate-dependent and fixed.

Simulation design We consider six scenarios, defined by combinations of copula families (Gaussian, Clayton, or Gumbel) and dependence specifications (constant or covariate-dependent copula parameters). The marginal specifications follow those in Sec. 2. For each setting, we consider sample sizes $n = 250, 500, 750$ and perform $R = 100$ replications. Spatial locations are sampled uniformly in $\mathcal{D} = [0, 1]^2$, using a fixed mesh with $M = 703$ nodes. Covariates are defined as $z_\beta(\mathbf{s}) = 2 \sin(2\pi s_1) \sin(4\pi s_2)$ for marginal means and $z_\kappa(\mathbf{s}) = 1/2 + \sin(2\pi s_1) \cos(4\pi s_2)$ for covariance components. In the *constant dependence* case, we set $\eta_\rho = 0.577$, yielding a target correlation parameter $\rho \approx 0.5$ for the Gaussian copula, $\rho \approx 1.781$ for the Clayton copula and $\rho \approx 2.781$ for the Gumbel copula. In the *covariate-dependent* scenario, we define $\eta_\rho(\mathbf{s}) \approx 0.577 - 0.374 z_\rho(\mathbf{s})$, where $z_\rho(\mathbf{s}) = \sin(4s_2 + s_1) - \frac{1}{2} \exp(-64s_1^2)$. The covariate surfaces are illustrated in Figure S4 of the SM.

Model estimation is conducted using a MCMC sampler with 15,000 iterations, burn-in of 7,000, and a thinning factor of 8. Each dataset is fitted using the true copula and the two alternatives.

The MCMC sampler is implemented in R. For the mesh construction and GMRF precision matrix calculations, R-INLA (Bakka et al., 2018) was used.

Results In the SM F, we report in the Table S4 the percentages of each selected model under different copula, sample size and type of dependence specification, while Figures S5, S6 and S7 in SM F, report the DIC values of the correctly specified model against its competitors. The corresponding WAIC results are not too far from DIC, and are shown . Points above the diagonal indicate a preference for the true model.

If the Gaussian copula is the correct model (Figure S5), the DIC is able to select the true copula for all sample sizes for varying values of the correlation parameter. However, for constant correlation, it is more difficult for the DIC to decide between the Clayton and the Gaussian copula, as in some replications the Gumbel model yields smaller DIC values compared to the true model. For increasing sample sizes, the problem vanishes.

If the Clayton copula is the correct model (Figure S6), the DIC consistently favors the true copula under both constant and varying dependence, with robustness across all sample sizes. The greatest differences in favor of the correct model are observed when the competitor is the Gumbel copula, which is easily explainable due to their different tail dependencies.

If the Gumbel copula is the correct model (Figure S7), even at smaller sample sizes, the DIC reliably selects the correct model. For a small sample size $n = 250$, only in a few replications for varying ρ , the Gaussian copula yields slightly smaller DIC values. Differences are larger when the Clayton copula is incorrectly assumed, because of its different tail dependencies.

In conclusion, the DIC and WAIC (SM F) are generally effective in identifying the appropriate copula family. The asymmetric copulas, such as Gumbel and Clayton, are more easily distinguished than the Gaussian copula due to their tail properties. The latter is slightly more challenging to identify in scenarios with constant or low correlation and small sample sizes.

5 Application to wind behaviour in Germany

We apply the proposed PWC model to wind data in Germany. Wind direction, measured in radians on $[0, 2\pi]$, indicates the angle of origin. Wind speed, recorded in m/s, typically ranges in $(0, 31.5]$, under non-hurricane conditions, according to the Beaufort Wind Scale. German wind patterns are mainly shaped by prevailing westerlies from the Atlantic Ocean, with additional easterly currents entering from Poland and the Czech Republic. Their interaction generates variability in northern Germany, whereas the complex orography in central and southern regions (e.g., the Harz Mountains, Black Forest, Bavarian Alps) produces local wind systems and turbulence. Coastal and northern plains typically exhibit higher wind speeds, reflecting the spatial constraints imposed by geography. Given the periodic and spatially correlated nature of the data, we apply the PWC model to analyze wind direction and speed jointly. This approach captures conditional dependence, incorporates covariates in the entire distribution, and accounts for spatial effects via nonstationary Matérn fields.

Data The data used for this application are obtained from the Deutscher Wetterdienst (DWD), and consist of hourly mean wind observations from 289 weather stations distributed across Germany. This dense network spans diverse geographic settings, enabling the assessment of both large-scale atmospheric dynamics and local effects. Alongside wind speed and direction, additional covariates are available, including visibility range, soil temperature (at a 5cm depth), vapor pressure, air pressure, wet bulb temperature, air temperature (at 2m), relative humidity, lower boundary height, and station altitude. These variables provide valuable explanatory information for structured additive predictors in our model. During storm periods, wind directions tend to be relatively homogeneous across the domain, whereas in calm weather they exhibit greater variability and more frequent directional shifts. We focus on a stormy weather episode between January 24th and 29th, 2025, and consider, for each station, the circular mean wind direction and the mean wind speed derived from the hourly data. As shown in Figure 2, the average wind direction was predominantly from the south and west, with a few locations across the country exhibiting mean wind speeds above 10 m/s. The wind rose confirms the dominance of westerly winds, with limited directional variability. These patterns are consistent with the passage of large-scale Atlantic frontal systems, which typically generate strong, persistent westerly flows across Central Europe during storm events.

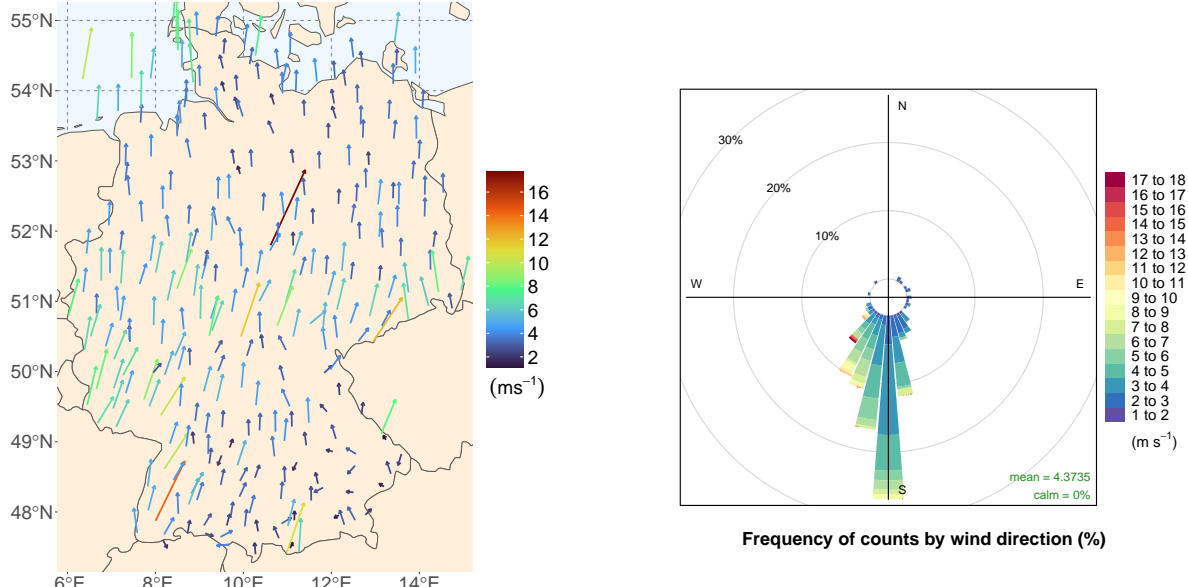


Figure 2: Wind behaviour in Germany during a storm weather period (24–29 January 2025). Left: station-wise average wind direction and mean wind speed (m/s), with arrow orientation indicating direction and colour scale representing speed. Right: wind rose summarizing the frequency distribution of directions the winds blew from across all stations, with colours denoting wind speed classes.

Model specification To investigate the relation between wind direction and speed for these data, we fit our PWC model with wrapped normal and lognormal margins as in (4) and (5), by

initially including all the covariates for both the two marginal models and for the copula. In Figure S11 of the SM, we show randomized quantile residuals via the inverse CDF of a standard normal distribution, suggested by Klein et al. (2015) as a simple and effective diagnostic to evaluate the fit of the marginal distributions. If the models are correctly specified, the residuals should follow approximately a standard normal distribution in Figure S11 of the SM.

For wind speed, the log-normal model estimated in the first stage provides an excellent fit to the data. For the circular variable wind direction, the wrapped normal distribution offers a reasonable fit, although it shows some difficulty in capturing the overall shape of the distribution, resulting in slight sigmoidal deviations from the diagonal. Nevertheless, note that the reported values for the circular distribution are only an approximation of the estimated PDF, for specific values of winding numbers, and the tails could be affected by this approximation. Thus, we retain the wrapped normal margin, recalling that our focus lies on the benefits of including a covariate-dependent dependence structure into the model rather than assuming independent marginals, and on exploring alternative forms of dependence beyond the symmetric dependence and linear correlation.

Selection of covariates in the marginal models is guided by the DIC and WAIC, comparing different predictor specifications (Klein and Kneib, 2016b). In the second stage, we analogously examine the role of covariates in the dependence structure induced by the copula. Specifically, for each copula family, constant and covariate-dependent specifications for the copula parameter are compared using DIC and WAIC. In particular, we compare the Gaussian copula (N), which exhibits no tail dependence, with the Clayton copula (C), which captures lower-tail dependence, and the Gumbel copula (G), which captures upper-tail dependence. In addition, we assess the sensitivity of dependence modeling under possible misspecification.

Predictive performance To further compare competing copula specifications in terms of copula family and in terms of constant or covariate-dependent copula parameter, We assess predictive performances for the models after variable selection based on DIC and WAIC. We use proper scoring rules based on ten-fold cross-validation, with observations randomly assigned to folds. We consider the logarithmic score (nLS), the energy score (ES), and a cylindrical definition of the continuous ranked probability score ($CRPS_{cyl}$), which extends the ES to the cylindrical domain. Lower scores indicate higher predictive accuracy.

5.1 Results

Selecting the dependence structure The model comparison results in Table 1 confirm that accounting for dependence substantially improves the model fit. Both DIC and WAIC favor copula-based models over the independence assumption, with further improvement when covariate effects are introduced in the copula parameter. Probabilistic forecasts are assessed through the scoring rules nLS, ES, and $CRPS_{cyl}$. In line with the criteria, including covariates in the dependence structure, the model's scores decrease, thereby delivering a better forecast. The Gumbel copula with covariate-dependent parameter (G1) yields the lowest information criteria and best predictive scores across all metrics, indicating the presence of upper-tail dependence between wind direction and speed

in this specific storm episode. The initially observed lower-tail pattern under the Clayton copula disappears once covariates are included, suggesting that it was primarily explained by the effects of meteorological covariates rather than true lower-tail asymmetry. Consequently, the subsequent results presented are based on the best performing model G1.

Table 1: Model comparison based on information criteria (computed based on the complete dataset, using the selected covariates) and average predictive scores (based on ten-fold cross-validation) for the independent model (I), copula models with constant parameter (0), and covariate-dependent parameter (1). Lower values indicate better performance.

Model	DIC	WAIC	nLS	ES	CRPS _{cyl}	AS	RMSE
I	218.460	223.390	2.773	1.211	0.440	0.183	1.222
N0	208.080	214.490	2.821	1.211	0.493	0.183	1.223
C0	206.890	212.450	2.773	1.211	0.493	0.183	1.223
G0	210.830	217.500	2.802	1.211	0.493	0.182	1.223
N1	197.550	203.772	2.793	1.181	0.478	0.172	1.202
C1	195.172	200.085	2.723	1.203	0.480	0.173	1.220
G1	190.656	195.691	2.532	1.041	0.391	0.097	1.088

Estimated posterior effects Posterior mean estimates and 95% credible intervals for all G1 model coefficients are reported in Table 2. The coefficients show consistent meteorological patterns: higher air pressure is associated with lower wind speeds and altered wind directions, while higher air temperatures and relative humidity tend to increase wind speeds. The copula parameter ρ shows a positive association with air pressure and visual range, and a negative association with wet-bulb temperature and lower cloud boundary height, indicating stronger dependence under clearer and more stable atmospheric conditions. Spatial random-field parameters (bottom part of the table) reveal marked non-stationarity for the directional component.

Results for spatial prediction Spatial prediction results are illustrated in Figure 3. The left panel displays the Cartesian product of the marginal credible intervals (here corresponding to circular sectors) for predicted wind vectors during a storm event at test set locations. The joint credible intervals are strictly included in them. The rainbow arrows represent observed wind direction and speed, while the purple and violet arrows denote the 0.025 and 0.975 posterior quantiles, respectively. Most observed wind vectors lie within the predicted intervals, demonstrating reliable uncertainty quantification and good calibration. The model successfully captures the wind dynamics across northern and central Germany. In contrast, predictive performance deteriorates in the southern region, particularly near the Alps, where abrupt changes in wind patterns and orographic effects are more complex to capture with the current mesh resolution. A finer mesh in these areas would improve local spatial representation and reduce predictive bias. The right panel of Figure 3 shows posterior mean estimates of the copula parameter ρ , which exhibits a clear spatial gradient, with higher values in the north indicating stronger dependence between direction and speed. In

Table 2: Posterior means and 95% credible intervals (in square brackets) for the marginal and copula parameters in G1 model.

	ϑ_1 (direction)	ϑ_2 (speed)	ϑ_ρ (dependence)
Nugget variance	0.047 [0.029, 0.073]	0.072 [0.058, 0.088]	—
Intercept	3.216 [3.192, 3.242]	1.389 [1.358, 1.420]	-1.560 [-2.292, -1.005]
Visibility range	—	-0.125 [-0.173, -0.077]	1.212 [0.308, 1.951]
Soil temperature (5 cm)	0.011 [-0.040, 0.063]	0.277 [0.200, 0.348]	—
Vapor pressure	—	-0.195 [-0.337, -0.052]	—
Air pressure	-0.180 [-0.244, -0.116]	-0.342 [-0.399, -0.283]	2.375 [1.316, 3.464]
Air temperature (2 m)	0.192 [0.107, 0.271]	0.292 [0.132, 0.449]	—
Relative humidity	-0.049 [-0.113, 0.012]	0.211 [0.085, 0.337]	—
Lower boundary height	-0.182 [-0.221, -0.146]	—	-0.915 [-1.492, -0.318]
Wet-bulb temperature	—	—	-1.713 [-2.811, -0.489]
GMRF log-linear coefficients			
Intercept $\theta_{\tau,0}$	-6.543 [-7.397, -5.995]	-2.377 [-2.870, -1.779]	—
Intercept $\theta_{\kappa,0}$	5.074 [4.674, 5.572]	2.595 [1.783, 3.193]	—
Altitude $\theta_{\kappa,1}$	-0.914 [-1.235, -0.665]	0.047 [-0.256, 0.332]	—

comparison, lower values in the mountainous south reflect weaker or more variable associations, consistent with the increased turbulence typical of complex terrain.

6 Conclusion and outlook

We proposed the PWC model, a generalization of copula-based models for directional statistics that allows for flexible specification of the linear components and recovers the cylindrical joint

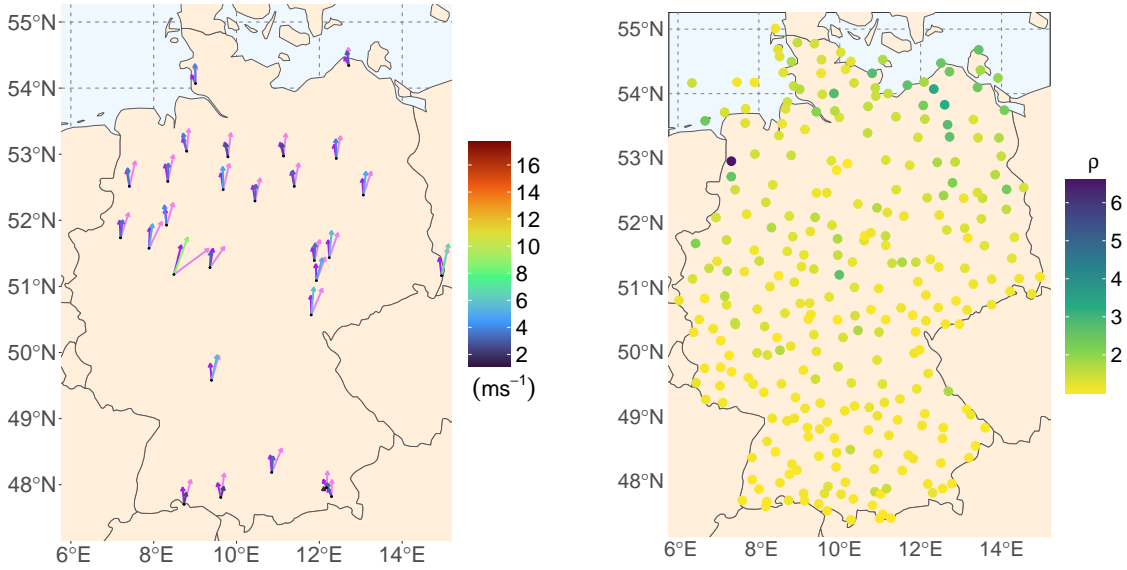


Figure 3: Left: credible intervals for wind vectors at test locations during a storm period. The rainbow arrows indicate the observed wind direction and speed, while the purple and violet arrows denote the 0.025 and 0.975 posterior quantiles, respectively. Right: posterior mean estimates of the copula parameter ρ at all locations.

model through a wrapping construction. The PWC model accommodates spatially correlated data by defining marginal models driven by non-stationary latent GRFs, and introduces a conditional copula regression framework linking the specified marginals. Additionally, we investigated the role of covariates in the dependence structure, showing that accounting for environmental variables in the association between wind speed and wind direction can substantially improve model fit.

Several extensions of the proposed framework are possible. For the marginal distributions, more flexible formulations may be adopted, such as the wrapped skew-normal (Mastrantonio et al., 2016) or wrapped mixtures (Greco et al., 2023) for the circular component, and the generalized gamma or Dagum distributions for the linear component. Furthermore, the copula governing the dependence structure could be made location-specific or replaced with alternatives based on trigonometric functions or semi-parametric formulations (Kauermann et al., 2013; Kuschinski and Jara, 2025) to capture more complex forms of association. Future work will focus on extending the model to a fully spatio-temporal framework, allowing dynamic dependence between circular and linear processes to be modeled over space and time.

References

Acar, E. F., R. V. Craiu, and F. Yao (2011). Dependence calibration in conditional copulas: a nonparametric approach. *Biometrics* 67(2), 445–453.

Bakka, H., H. Rue, G.-A. Fuglstad, A. Riebler, D. Bolin, J. Illian, E. Krainski, D. Simpson, and F. Lindgren (2018). Spatial modeling with R-INLA: a review. *Wiley Interdisciplinary Reviews: Computational Statistics* 10(6), e1443.

Bolin, D. and K. Kirchner (2020). The rational SPDE approach for Gaussian random fields with general smoothness. *Journal of Computational and Graphical Statistics* 29(2), 274–285.

Carta, J. A., P. Ramirez, and S. Velazquez (2009). A review of wind speed probability distributions used in wind energy analysis: case studies in the Canary Islands. *Renewable and Sustainable Energy Reviews* 13(5), 933–955.

Fahrmeir, L., T. Kneib, S. Lang, and B. D. Marx (2022). *Regression: Models, Methods and Applications*. Berlin Heidelberg: Springer.

Fernández-Durán, J. J. (2007, 01). Models for circular–linear and circular–circular data constructed from circular distributions based on nonnegative trigonometric sums. *Biometrics* 63(2), 579–585.

Gelman, A., W. R. Gilks, and G. O. Roberts (1997). Weak convergence and optimal scaling of random walk Metropolis algorithms. *Annals of Applied Probability* 7(1), 110–120.

Gelman, A., H. S. Stern, J. B. Carlin, D. B. Dunson, A. Vehtari, and D. B. Rubin (2013). *Bayesian Data Analysis* (3rd ed.). Boca Raton, FL: Chapman & Hall/CRC.

Greco, L., P. L. Novi Inverardi, and C. Agostinelli (2023). Finite mixtures of multivariate wrapped normal distributions for model based clustering of p-torus data. *Journal of Computational and Graphical Statistics* 32(3), 1215–1228.

Hodel, F. H. and J. R. Fieberg (2022). Circular–linear copulae for animal movement data. *Methods in Ecology and Evolution* 13(5), 1001–1013.

Ingebrigtsen, R., F. Lindgren, I. Steinsland, and S. Martino (2015). Estimation of a non-stationary model for annual precipitation in southern Norway using replicates of the spatial field. *Spatial Statistics* 14, 338–364.

Johnson, R. A. and T. E. Wehrly (1978). Some angular-linear distributions and related regression models. *Journal of the American Statistical Association* 73(363), 602–606.

Jona-Lasinio, G., A. Gelfand, and M. Jona-Lasinio (2012). Spatial analysis of wave direction data using wrapped Gaussian processes. *The Annals of Applied Statistics* 6(4), 1478–1498.

Jona-Lasinio, G., M. Santoro, and G. Mastrantonio (2020). Circspacetime: an R package for spatial and spatio-temporal modelling of circular data. *Journal of Statistical Computation and Simulation* 90(7), 1315–1345.

Jones, M. C., A. Pewsey, and S. Kato (2015). On a class of circulas: copulas for circular distributions. *Annals of the Institute of Statistical Mathematics* 67(5), 843–862.

Kauermann, G., C. Schellhase, and D. Ruppert (2013). Flexible copula density estimation with penalized hierarchical B-splines. *Scandinavian Journal of Statistics* 40(4), 685–705.

Klein, N. and T. Kneib (2016a). Scale-dependent priors for variance parameters in structured additive distributional regression. *Bayesian Analysis* 11, 1071–1106.

Klein, N. and T. Kneib (2016b). Simultaneous inference in structured additive conditional copula regression models: a unifying Bayesian approach. *Statistics and Computing* 26, 841–860.

Klein, N., T. Kneib, S. Lang, and A. Sohn (2015). Bayesian structured additive distributional regression with an application to regional income inequality in Germany. *The Annals of Applied Statistics* 9(2), 1024–1052.

Kurz, G., I. Gilitschenski, and U. D. Hanebeck (2014). Efficient evaluation of the probability density function of a wrapped normal distribution. In *2014 Sensor Data Fusion: Trends, Solutions, Applications (SDF)*, pp. 1–5. IEEE.

Kuschinski, N. and A. Jara (2025). Grid-uniform copulas and rectangle exchanges: Bayesian model and inference for a rich class of copula functions. *Bayesian Analysis* 20(1), 55–82.

Lagona, F. (2018). Correlated cylindrical data. In *Applied Directional Statistics*, pp. 61–76. Chapman and Hall/CRC.

Lagona, F. (2019). Copula-based segmentation of cylindrical time series. *Statistics & Probability Letters* 144, 16–22.

Lagona, F. and M. Mingione (2025). Nonhomogeneous hidden semi-Markov models for toroidal data. *Journal of the Royal Statistical Society Series C: Applied Statistics* 74(1), 142–166.

Lang, M. N., G. J. Mayr, R. Stauffer, and A. Zeileis (2019). Bivariate Gaussian models for wind vectors in a distributional regression framework. *Advances in Statistical Climatology, Meteorology and Oceanography* 5(2), 115–132.

Lindgren, F., H. Rue, and J. Lindström (2011). An explicit link between Gaussian fields and Gaussian Markov random fields: the stochastic partial differential equation approach. *Journal of the Royal Statistical Society: Series B* 73(4), 423–498.

Mardia, K. V. and P. E. Jupp (2000). *Directional Statistics*. Chichester: John Wiley & Sons.

Marques, I., T. Kneib, and N. Klein (2022). A non-stationary model for spatially dependent circular response data based on wrapped Gaussian processes. *Statistics and Computing* 32(5), 73.

Mastrantonio, G. (2022). Modeling animal movement with directional persistence and attractive points. *The Annals of Applied Statistics* 16(3), 2030–2053.

Mastrantonio, G., A. E. Gelfand, and G. Jona-Lasinio (2016). The wrapped skew Gaussian process for analyzing spatio-temporal data. *Stochastic Environmental Research and Risk Assessment* 30(8), 2231–2242.

Meilán-Vila, A., R. M. Crujeiras, and M. Francisco-Fernández (2021). Nonparametric estimation of circular trend surfaces with application to wave directions. *Stochastic Environmental Research and Risk Assessment* 35(4), 923–939.

Miller, D. L., R. Glennie, and A. E. Seaton (2020). Understanding the stochastic partial differential equation approach to smoothing. *Journal of Agricultural, Biological and Environmental Statistics* 25(1), 1–16.

Nelsen, R. (2006). *An Introduction to Copulas*. Portland: Springer.

Ogata, H. (2023). Copula bounds for circular data. In *Research Papers in Statistical Inference for Time Series and Related Models: Essays in Honor of Masanobu Taniguchi*, pp. 389–402. Springer.

Pewsey, A. and E. García-Portugués (2021). Recent advances in directional statistics. *TEST* 30, 1–58.

Simpson, D., H. Rue, A. Riebler, T. G. Martins, and S. H. Sørbye (2017). Penalising model component complexity: a principled, practical approach to constructing priors. *Statistical Science* 32(1), 1–28.

Spiegelhalter, D. J., N. G. Best, B. P. Carlin, and A. van der Linde (2002). Bayesian measures of model complexity and fit. *Journal of the Royal Statistical Society: Series B* 64(4), 583–639.

Tang, W., L. Zhang, and S. Banerjee (2021). On identifiability and consistency of the nugget in Gaussian spatial process models. *Journal of the Royal Statistical Society: Series B* 83(5), 1044–1070.

Vatter, T. and T. Nagler (2018). Generalized additive models for pair-copula constructions. *Journal of Computational and Graphical Statistics* 27(4), 715–727.

Vehtari, A., A. Gelman, and J. Gabry (2017). Practical Bayesian model evaluation using leave-one-out cross-validation and WAIC. *Statistics and Computing* 27(5), 1413–1432.

Vihola, M. (2012). Robust adaptive Metropolis algorithm with coerced acceptance rate. *Statistics and Computing* 22(5), 997–1008.

Watanabe, S. and M. Opper (2010). Asymptotic equivalence of Bayes cross validation and widely applicable information criterion in singular learning theory. *Journal of Machine Learning Research* 11, 3571–3594.

Wood, S. N. (2017). *Generalized additive models: an introduction with R.* Chapman & Hall/CRC.

Supplementary Material

A Theoretical results and proofs

A.1 Details on $p_{1,2}^{\text{PW}}$

The joint density $p_{1,2}^{\text{PW}}(\varphi_1, y_2 | \mathbf{z})$ is well-defined as it satisfies the standard requirements for a valid probability density function.

First, the total integral over the cylindrical domain equals one:

$$\int_{-\infty}^{+\infty} \int_0^{2\pi} p_{1,2}^{\text{PW}}(\varphi_1, y_2 | \mathbf{z}) d\varphi_1 dy_2 = 1,$$

which follows directly from Lemma 1 and the fact that the wrapped marginal integrates the unwrapped joint density over the infinite lattice of 2π -shifts.

Second, non-negativity is ensured since $p_{1,2}^{\text{PW}}$ is defined as a countable sum of non-negative terms, each being the evaluation of a Euclidean joint density:

$$p_{1,2}^{\text{PW}}(\varphi_1, y_2 | \mathbf{z}) = \sum_{k \in \mathbb{Z}} p_{1,2}(\varphi_1 + 2\pi k, y_2 | \mathbf{z}) \geq 0.$$

Third, $p_{1,2}^{\text{PW}}$ satisfies 2π -periodicity in the circular component. For all $j \in \mathbb{Z}$, we have:

$$\begin{aligned} p_{1,2}^{\text{PW}}(\varphi_1 + 2\pi j, y_2 | \mathbf{z}) &= \sum_{k \in \mathbb{Z}} p_{1,2}(\varphi_1 + 2\pi j + 2\pi k, y_2 | \mathbf{z}) \\ &= \sum_{h \in \mathbb{Z}} p_{1,2}(\varphi_1 + 2\pi h, y_2 | \mathbf{z}) \\ &= p_{1,2}^{\text{PW}}(\varphi_1, y_2 | \mathbf{z}), \end{aligned}$$

where the index substitution $h = j + k$ justifies equality.

Hence, $p_{1,2}^{\text{PW}}$ is a valid cylindrical probability density function.

A.2 Proof of Lemma 1

Proof. Marginalization of the circular part $\int_0^{2\pi} p_{1,2}^{\text{PW}}(\varphi_1, y_2 | \mathbf{z}) d\varphi_1$ yields

$$\begin{aligned} &\int_0^{2\pi} \sum_{k \in \mathbb{Z}} c(F_1(\varphi_1 + 2\pi k | \mathbf{z}), F_2(y_2 | \mathbf{z}) | \mathbf{z}) p_1(\varphi_1 + 2\pi k | \mathbf{z}) p_2(y_2 | \mathbf{z}) d\varphi_1 \\ &\stackrel{(a)}{=} \sum_{k \in \mathbb{Z}} \int_0^{2\pi} c(F_1(\varphi_1 + 2\pi k | \mathbf{z}), F_2(y_2 | \mathbf{z}) | \mathbf{z}) p_1(\varphi_1 + 2\pi k | \mathbf{z}) p_2(y_2 | \mathbf{z}) d\varphi_1 \\ &\stackrel{(b)}{=} \int_{-\infty}^{+\infty} c(F_1(y_1 | \mathbf{z}), F_2(y_2 | \mathbf{z}) | \mathbf{z}) p_1(y_1 | \mathbf{z}) p_2(y_2 | \mathbf{z}) dy_1 \\ &\stackrel{(c)}{=} p_2(y_2 | \mathbf{z}). \end{aligned}$$

Marginalization of the linear part $\int_{-\infty}^{\infty} p_{1,2}^{PW}(\varphi_1, y_2 \mid \mathbf{z}) dy_2$ yields

$$\begin{aligned}
& \int_{-\infty}^{\infty} \sum_{k \in \mathbb{Z}} c(F_1(\varphi_1 + 2\pi k \mid \mathbf{z}), F_2(y_2 \mid \mathbf{z}) \mid \mathbf{z}) p_1(\varphi_1 + 2\pi k \mid \mathbf{z}) p_2(y_2 \mid \mathbf{z}) dy_2 \\
& \stackrel{(a)}{=} \sum_{k \in \mathbb{Z}} \int_{-\infty}^{\infty} c(F_1(\varphi_1 + 2\pi k \mid \mathbf{z}), F_2(y_2 \mid \mathbf{z}) \mid \mathbf{z}) p_1(\varphi_1 + 2\pi k \mid \mathbf{z}) p_2(y_2 \mid \mathbf{z}) dy_2 \\
& \stackrel{(c)}{=} \sum_{k \in \mathbb{Z}} p_1(\varphi_1 + 2\pi k \mid \mathbf{z}) \\
& = p_1^W(\varphi_1 \mid \mathbf{z}).
\end{aligned}$$

At (a), we use the dominated convergence theorem, at (b) we use the concatenation of integrals, and at (c) Sklar's theorem. \square

B Summary on copula specifications

Table S3: Considered one-parameter copula functions with their admissible range for the association parameter ρ and the corresponding link function. Here, $\Phi_2(\cdot, \cdot; \rho)$ denotes the CDF of a standard bivariate Gaussian distribution with correlation coefficient ρ , and $\Phi(\cdot)$ denotes the CDF of a standard univariate Gaussian distribution.

Copula	$C(u_1, u_2; \rho)$	Range of ρ	Link function
Gaussian	$\Phi_2(\Phi^{-1}(u_1), \Phi^{-1}(u_2); \rho)$	$[-1, 1]$	$\frac{\rho}{\sqrt{1 - \rho^2}}$
Clayton	$(u_1^{-\rho} + u_2^{-\rho} - 1)^{-1/\rho}$	$(0, \infty)$	$\log(\rho)$
Gumbel	$\exp\left[-\left\{\left(-\log u_1\right)^\rho + \left(-\log u_2\right)^\rho\right\}^{1/\rho}\right]$	$(1, \infty)$	$\log(\rho - 1)$

C Details on MCMC sampler

C.1 Full conditionals for Gibbs sampler

Let's consider a vector of Gaussian observations $\mathbf{y} = (y_1, \dots, y_n)^\top$, and likelihood with mean parameters $\{\mu_i\}_{i=1}^n$ and variances σ^2 , and a generic mean predictor

$$\boldsymbol{\eta}_{\boldsymbol{\mu}} = Z_0\beta_0 + Z_1\boldsymbol{\beta}_1 + \dots + Z_J\boldsymbol{\beta}_J,$$

where $Z_0 = \mathbf{1}$ is the unit vector, β_0 denotes the intercept, Z_j a generic design matrix, related to some effects, and $\boldsymbol{\beta}_j$ is the corresponding parameter vector. For all mean coefficients endowed with Gaussian (N) priors (e.g., $\beta_0 \sim N(0, a_0)$ and $\boldsymbol{\beta}_j \mid \xi_j^2 \sim N(0, \xi_j^2 \mathbf{I})$) and Inverse Gamma (IG) priors for the variance (e.g., $\sigma^2 \sim IG(0.001, 0.001)$), full conditional updates can be derived analytically.

In particular, the product of two Gaussian densities is proportional to a Gaussian density, which implies conjugacy and leads to closed-form full conditional distributions. (see, e.g., Fahrmeir et al., 2022). Exploiting this result, we obtain the following general full conditional forms:

$$\begin{aligned}\beta_j | \cdot &\sim \mathcal{N}\left((E + F)^{-1}(E\mathbf{e} + F\mathbf{f}), (E + F)^{-1}\right), \\ \sigma^2 | \cdot &\sim \text{IG}\left(0.001 + \frac{n}{2}, 0.001 + \frac{1}{2}(\mathbf{y} - \boldsymbol{\eta}_\mu)^\top(\mathbf{y} - \boldsymbol{\eta}_\mu)\right).\end{aligned}$$

where $E = \frac{1}{\sigma^2} Z_j^\top Z_j$ collects the information from the Gaussian likelihood, $F = 1/\xi^2 \mathbf{I}$ (or $F = 1/a_0$ for the intercept parameter) encodes the corresponding Gaussian prior contribution, $\mathbf{e} = Z_j^\top (Z_j Z_j^\top)^{-1}(\mathbf{Y} - \boldsymbol{\eta}_\mu + Z_j \boldsymbol{\beta}_j)$ and $\mathbf{f} = \mathbf{0}$.

C.2 Gaussian Markov random field precision matrix

For a stationary GRF solution to the SPDE, the GMRF precision is

$$Q = \tau (\kappa^4 C + 2\kappa^2 G + G C^{-1} G),$$

where C and G are FEM mass and stiffness matrices, respectively.

With spatially varying $\kappa(\mathbf{s})$, using mass lumping so C is diagonal:

$$Q = \tau (\text{diag}(\kappa)^2 C \text{diag}(\kappa)^2 + \text{diag}(\kappa)^2 G + G' \text{diag}(\kappa)^2 + G C^{-1} G) \tau.$$

D Penalized Complexity Priors for variances

Penalized Complexity (PC) priors (Simpson et al., 2017) formalize Occam’s razor by shrinking toward a *base model* and penalizing deviations from it at a constant rate. For variance components, the base model is the ”no-variance” model (random–effect variance equal to zero).

Occam’s razor A simpler model formulation (base model) should be preferred until there is enough support for a more complex model.

Measure of complexity Let $p = p(y | \xi)$ denote the likelihood under parameter ξ (e.g., a variance or standard deviation) and let $p_0 = p(y | \xi_0)$ be the likelihood under the base model. Define the unidirectional distance from the base model via the Kullback–Leibler divergence (KLD):

$$d(\xi) = \sqrt{2 \text{KLD}(p \| p_0)}, \text{ where } \text{KLD}(p \| q) = \int p(u) \log\left(\frac{p(u)}{q(u)}\right) du.$$

Here $d(\xi) \geq 0$ and $d(\xi_0) = 0$. Larger d means greater deviation from the simpler model.

Constant rate penalization PC priors assume an exponential law on the distance scale,

$$\pi_d(d) = \lambda \exp(-\lambda d), \quad d \geq 0,$$

which yields (by change of variables) the prior on ξ :

$$\pi(\xi) = \lambda \exp(-\lambda d(\xi)) \left| \frac{d}{d\xi} d(\xi) \right|.$$

This places maximal prior mass at the base model and yields exponentially decreasing weight for more complex models.

User-defined scaling (tail calibration) The rate λ is fixed by a simple tail-probability statement reflecting a sensible scale for the parameter. Once $U > 0$ as a “sensible”, user-defined upper bound that specifies the prior knowledge about “tail events” and $\alpha \in (0, 1)$ as the weight to put on this event, are chosen, the condition $\mathbb{P}(Q(\xi) > U) = \alpha$ is imposed for a monotone scale function Q , which is an interpretable transformation of the flexibility parameter. This condition allows the user to prescribe how informative the resulting PC prior shall be.

E Details on model choice

The DIC and WAIC are simulation-based criteria, which are straightforward to compute from MCMC output and have been widely used for comparing response distributions and predictor specifications, in a stepwise model choice strategy. The DIC combines a measure of model fit, given by the average deviance across posterior draws $\overline{D(\vartheta)}$, with a penalty for model complexity, defined as the difference between the mean deviance and the deviance at a representative point of the posterior (e.g., the posterior mean) $D(\bar{\vartheta})$. The criterion is formally defined as $\text{DIC} = \frac{2}{T} \sum D(\vartheta^{[t]}) - D(\frac{1}{T} \sum \vartheta^{[t]})$ where $D(\vartheta) = -2 \log p(y | \vartheta)$.

The WAIC provides a fully Bayesian alternative, based on the log-pointwise predictive density $\text{lppd} = \sum_{i=1}^n \log \int p(y_i | \vartheta) p(\vartheta | y) d\vartheta$ with a complexity penalty given by the variance of the log-likelihood across posterior draws and summed over data points $\text{pWAIC} = \sum_{i=1}^n 2 \text{var}_{\vartheta}(\log p(y_i | \vartheta))$, (Gelman et al. (2013); Vehtari et al. (2017)), yielding to $\text{WAIC} = -2(\text{lppd} - \text{pWAIC})$. The WAIC is invariant to parameterization, robust in the presence of skewed or multimodal posteriors, while the DIC may be sensitive when posterior distributions deviate from normality. Since both are sample-based, slight differences between competing models may lead to a region of indecisiveness; however, the criteria have been shown to favor sparser models when combined with the exclusion of effects whose credible intervals include zero. Simulation studies in Klein et al. (2015) further suggest that the DIC effectively detect omitted relevant covariates, while the inclusion of irrelevant ones usually results only in insignificant effects.

F Simulation study

We report here the table and figures discussed in Sec. 4.

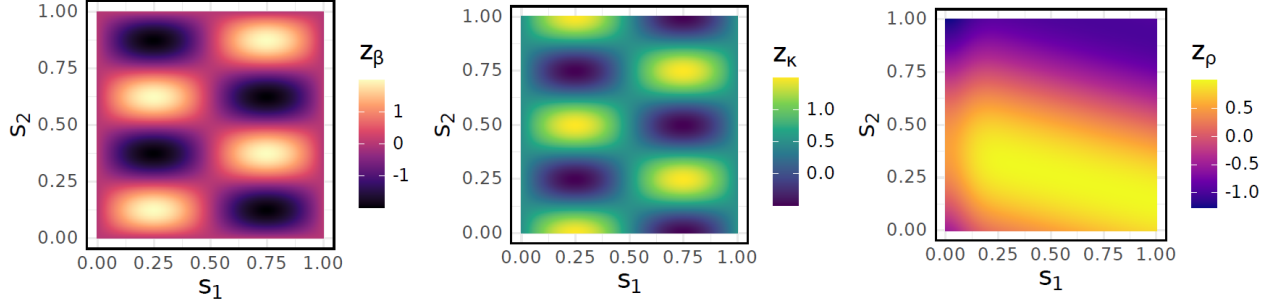


Figure S4: The three boxes show, from left to right, the covariates functions $z_\beta(\mathbf{s}) = 2 \sin(2\pi s_1) \sin(4\pi s_2)$, $z_\kappa(\mathbf{s}) = 1/2 + \sin(2\pi s_1) \cos(4\pi s_2)$, and $z_\rho(\mathbf{s}) = \sin(4*s_2 + s_1) - \frac{1}{2} \exp(-64s_1^2)$ used in the simulation study.

Table S4: Percentage of replications with minimum DIC among the three investigated copula models. Columns report combinations of the true copula model under which data were generated and sample size n , while the rows show the fitted copula model (N=“Gaussian”, C=“Clayton”, G=“Gumbel”), with a constant or covariate-dependent (varying) copula dependence parameter ρ .

DIC	Clayton			Gumbel			Gaussian		
	$n=250$	$n=500$	$n=750$	$n=250$	$n=500$	$n=750$	$n=250$	$n=500$	$n=750$
constant ρ	C	100	100	100	0	0	0	5	0
	G	0	0	0	100	100	100	21	29
	N	0	0	0	0	0	74	71	87
varying ρ	C	100	100	100	0	0	0	0	0
	G	0	0	0	94	100	99	0	0
	N	0	0	0	6	0	1	100	100

We report the empirical evaluations for comparing DIC values under the true model and the other two competitors.

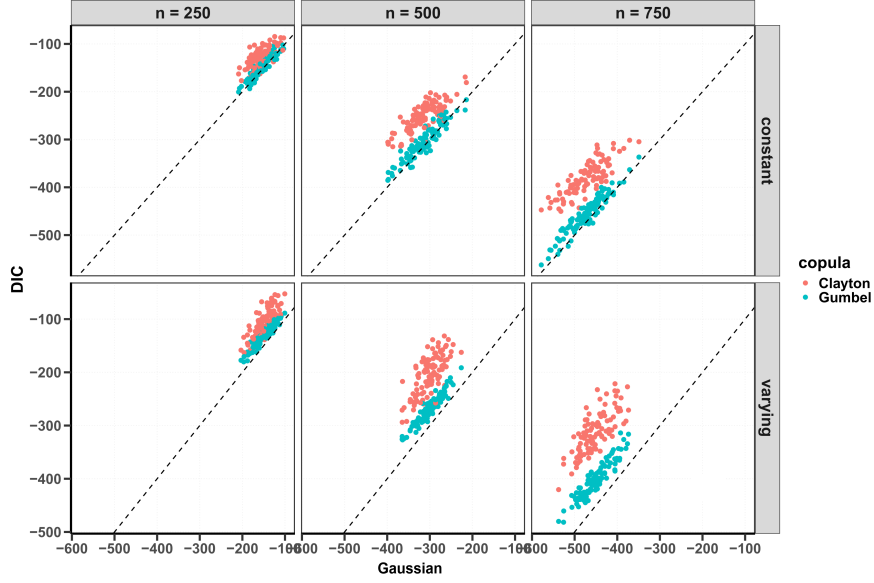


Figure S5: Comparison of DIC values under the correctly specified Gaussian copula model against the misspecified Clayton and Gumbel copula models. Columns correspond to sample sizes $n = 250, 500, 750$, while rows display the two dependence scenarios: **constant** copula parameter ρ , and **varying** ρ (covariate-dependent ρ).

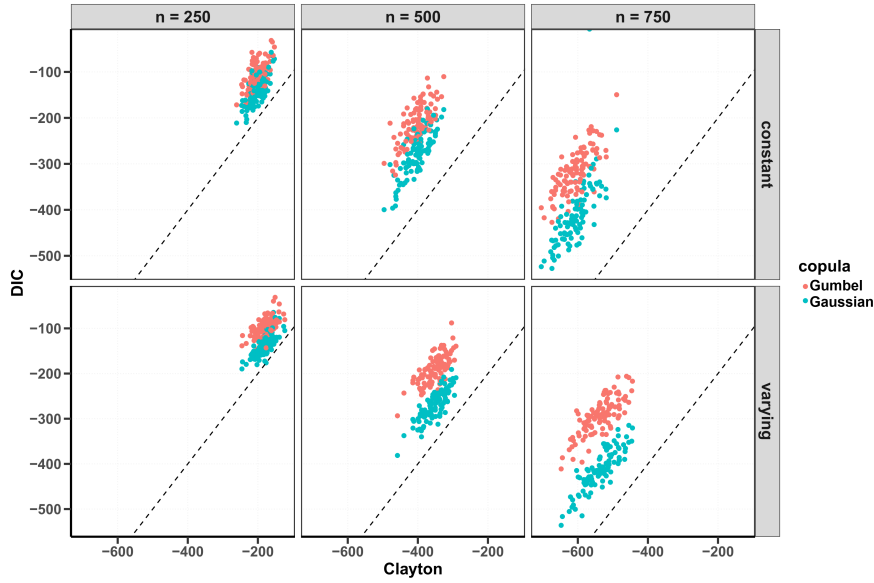


Figure S6: Comparison of DIC values under the correctly specified Clayton copula model against the misspecified Gaussian and Gumbel copula models. Columns correspond to sample sizes $n = 250, 500, 750$, while rows display the two dependence scenarios: **constant** copula parameter ρ , and **varying** ρ (covariate-dependent ρ).

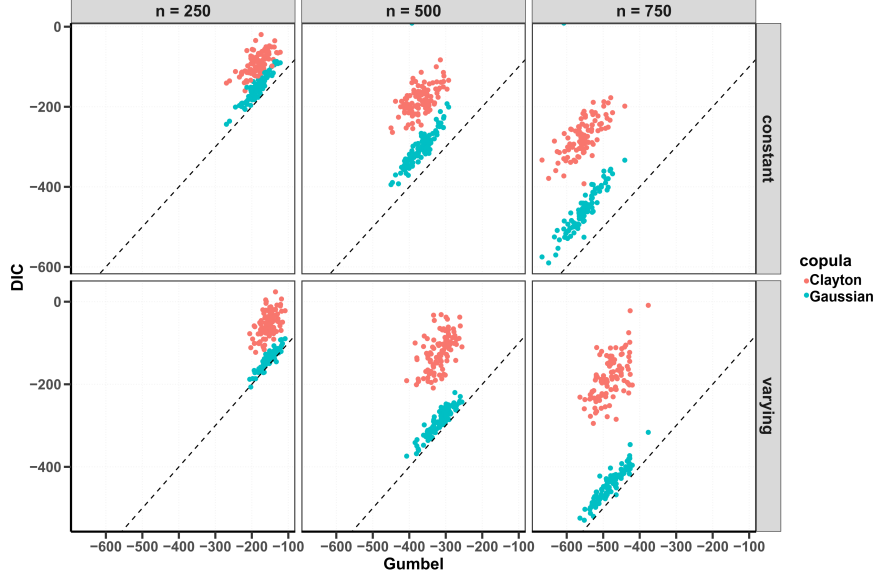


Figure S7: Comparison of DIC values under the correctly specified Gumbel copula model against the misspecified Gaussian and Clayton copula models. Columns correspond to sample sizes $n = 250, 500, 750$, while rows display the two dependence scenarios: **constant** copula parameter ρ , and **varying** ρ (covariate-dependent ρ).

We report the empirical evaluations for comparing WAIC values under the true model and the other two competitors.

Table S5: Percentage of replications with minimum WAIC among the three investigated copula models. Columns report combinations of the true copula model under which data were generated and sample size n , while the rows show the fitted copula model (N="Gaussian", C="Clayton", G="Gumbel"), with a constant or covariate-dependent (varying) copula dependence parameter ρ .

WAIC	Clayton			Gumbel			Gaussian			
	$n=250$	$n=500$	$n=750$	$n=250$	$n=500$	$n=750$	$n=250$	$n=500$	$n=750$	
constant ρ	C	100	100	100	0	0	0	6	3	0
	G	0	0	0	100	100	100	47	51	51
	N	0	0	0	0	0	0	47	46	49
varying ρ	C	100	100	100	0	0	0	0	0	0
	G	0	0	0	96	100	100	0	0	0
	N	0	0	0	4	0	0	100	100	100

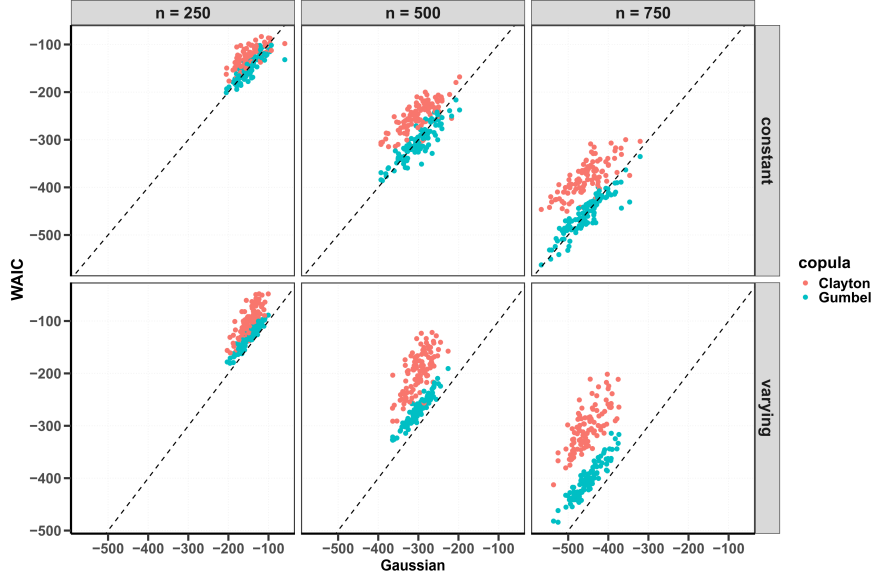


Figure S8: Comparison of WAIC values under the correctly specified Gaussian copula model (x-axis) against the misspecified Clayton and Gumbel copula models (y-axis). Columns correspond to increasing sample sizes $n = 250, 500, 750$, while rows display the two dependence scenarios: **constant**, with a constant copula parameter ρ , and **varying**, where ρ depends on a covariate.

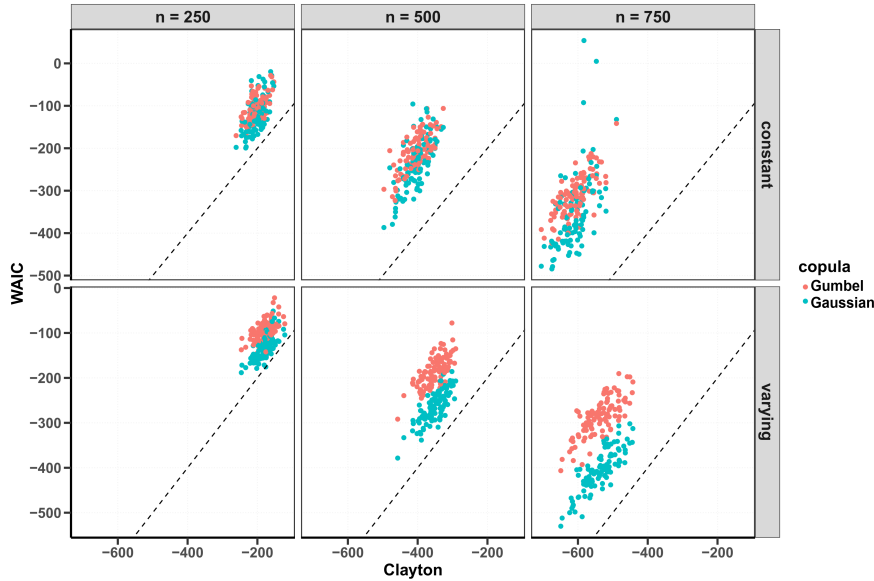


Figure S9: Comparison of WAIC values under the correctly specified Clayton copula model (x-axis) against the misspecified Gumbel and Gaussian copula models (y-axis). Columns correspond to increasing sample sizes $n = 250, 500, 750$, while rows display the two dependence scenarios: **constant**, with a constant copula parameter ρ , and **varying**, where ρ depends on a covariate.

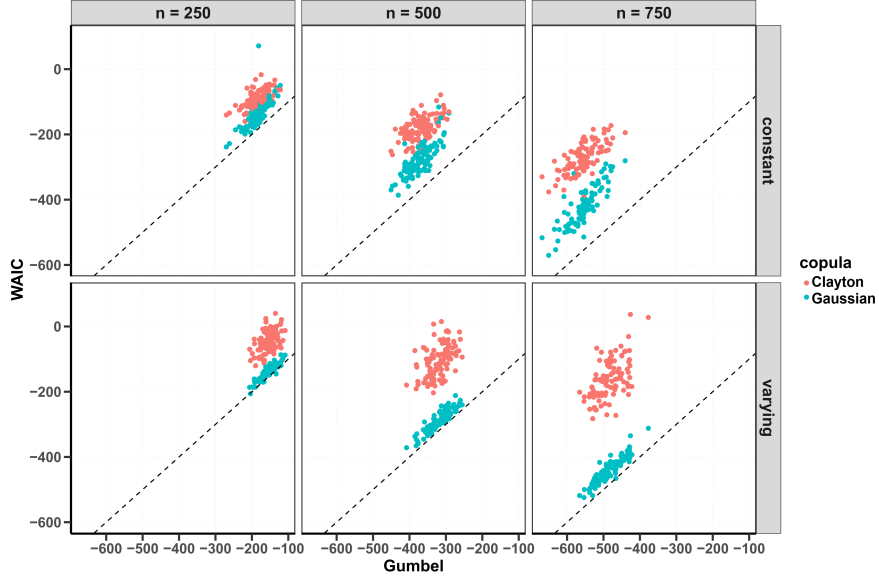


Figure S10: Comparison of WAIC values under the correctly specified Gumbel copula model (x-axis) against the misspecified Clayton and Gaussian copula models (y-axis). Columns correspond to increasing sample sizes $n = 250, 500, 750$, while rows display the two dependence scenarios: **constant**, with a constant copula parameter ρ , and **varying**, where ρ depends on a covariate.

G Supplementary details for Section 5

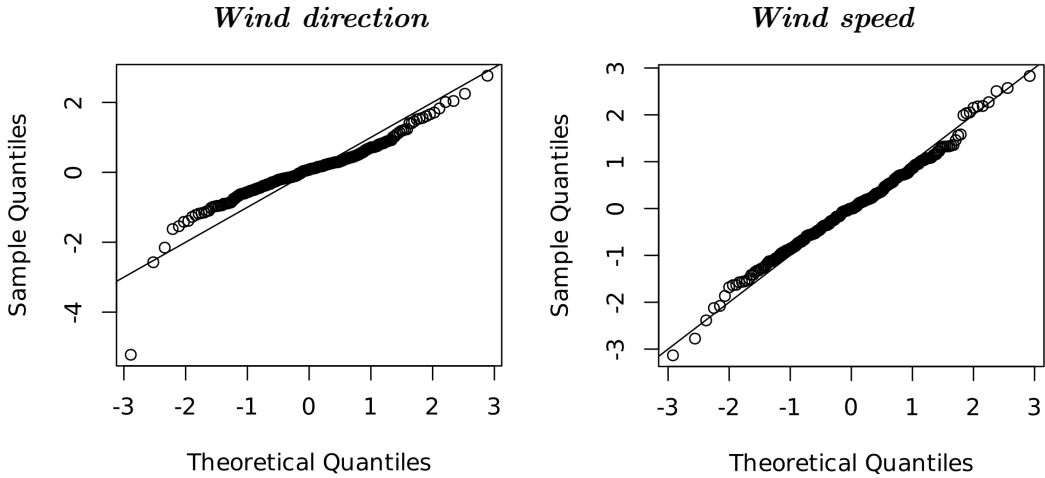


Figure S11: Randomized quantile residuals for the marginal models, corresponding to the linear model (left) for the wind speed and the circular model (right) for the wind direction.